Exploring the NLO Properties of Theoretically Designed Cu/Ag/Au-Doped C_3N_4 Systems through DFT Analysis

[1]Sehrish Gul, [1,2]Javed Iqbal*, [1]Ijaz Ahmad Bhatti and [1]Muhammad Asghar
[a]*Department of Chemistry, University of Agriculture, Faisalabad 38000, Pakistan*.
[b]*Department of Chemistry, College of Science, University of Bahrain, Sakhir, 32038, Kingdom of Bahrain.*
Javed.Iqbal@uaf.edu.pk; Jiqbal@uob.edu.bh*

(Received on 5th March 2025, accepted in revised form 5th August 2025)

Summary: Herein to explore nonlinear optical (NLO) properties, nine novel C_3N_4-based compounds have been theoretically developed through doping approach with coinage metals: copper (Cu), silver (Ag), and gold (Au). Every metal series has included three variations containing two, three, or four dopant atoms: (C_3N_4@2Cu, C_3N_4@3Cu, C_3N_4@4Cu, C3N4@2Ag, C3N4@3Ag, C3N4@4Ag, C3N4@2Au, C3N4@3Au, C3N4@4Au). These theoretically design model systems have been investigated with density functional theory (DFT) at the B3LYP/LANL2DZ level to study their electrical, optical, and NLO characteristics. Doping of C_3N_4 with coinage metals (Cu, Ag, Au) led to a noticeable improvement in their optical and electronic characteristics. The pure C_3N_4 material showed a relatively wide band gap (3.50 eV), an absorption maximum at 383 nm, and lower values of polarizability (α_0 = 479.00 au) and hyperpolarizability (β_0 = 479.10 au). After doping with coinage metals, all doped structures of C_3N_4 showed a redshift in absorption (λmax = 438–836 nm), narrow band gaps (0.63–2.29 eV), and lower excitation energies (ΔE = 1.39–2.99 eV). Additionally, the doped systems of C_3N_4 reveal higher transition dipole moments ($\Delta\mu$).), static mean polarizability ($\boldsymbol{\alpha_0}$) lies from 541.81 to 809.99 au, mean first hyperpolarizability ($\boldsymbol{\beta_0}$) ranges from 717.45 to 140245.86 au, isotropic (α_{iso}) polarizabilities (541.81-809.99 au) and anisotropic (α_{aniso}) polarizabilities (407.40-1298.65 au). This project will contribute to the development of theoretically design compounds with excess of electrons. The results of this investigation might affect forthcoming studies on exceptionally well NLO materials and act as valuable benchmarks for chemical compound synthesis.

Keywords: Carbon Nitride (C_3N_4); Coinage metals (Cu, Ag, Au); DFT; Hyperpolarizability.

Introduction

The swift development of optoelectronic and photonic technology has resulted in an increasing need for materials with superior nonlinear optical (NLO) capabilities. These materials are critical for the development of high-speed optical switches, optical limiters, and frequency converters, all of which are required components in modern telecommunications, data storage, and optical computing systems [1-5]. Organic, inorganic, and organometallic along with hybrid forms have been commercialized [6-8].

Materials with strong non-linear optical responses have been produced by employing different approaches namel, diradical character [9], D-A-π bridge system [10], and octupolar molecules [11]. Bond length alteration (BLA) theory, doping of metal atoms, and other techniques have been used to create outstanding NLO materials [12-18]. Doping is a viable approach to increase the NLO response by lowering transition energy followed by charge transfer in organic and inorganic systems [19-24].

In this context, Carbon nitride (C_3N_4), a 2D material with a graphene-like structure, exhibiting unique opt-electronic features has emerged as promising candidate, which can be tailored for specific applications. This stable layered material is built of a CN framework and closely mimics a graphitic nanostructure. This motivated the researchers to devote a great deal of time and effort to studying C_3N_4. As a result, they acquired extensive fundamental knowledge and wrote a number of studies on a variety of subjects, encompassing CN biosynthesis, composition and applications [25, 26]. C_3N_4 has been a polymeric, UV visible light-active photo catalyst having a bandgap of 2.7 eV (460 nm). Owing to its straightforward, affordable, environmentally friendly methods of preparation, potential stability and potent physicochemical properties for use in several applications, C_3N_4 has grown in importance in fields such as chemistry, physics, and technology. In contrast towards other semiconductors, C_3N_4 is simple to synthesis using a variety of techniques, has desirable electrical and morphological properties, and has good thermal stability even at 600 °C in the atmosphere [27, 28].

Coinage metals (Cu, Au, Ag) serve as especially intriguing dopants because of their tendency to create substantial interactions with the

*To whom all correspondence should be addressed.

C_3N_4 lattice, resulting in major alterations in its electrical and optical characteristics. These interactions can boost NLO responses, making metal-doped C_3N_4 an appealing choice for use in optical electronics. Several attempts to develop stable metallic clusters (Au, Ag, and Cu) of groups IB have used graphene and graphene-like materials. Metal impurities (Cu, Ag, and Au) are frequently added to increase binding function, resulting in a doped system with improved photocatalytic characteristics, leading to the narrowing of the energy difference between frontier molecular orbitals and enhancing the photocatalytic efficiency, physicochemical characteristics and visible absorption coefficient [29].

Numerous recent studies have been reported to support the enhanced optical activity in Au- & Ag-doped C_3N_4 systems, characteristically observing modest decrease in bandgap and enhancements in light absorption. Metal doping in C_3N_4 materials to enhance their optoelectronic and NLO properties. Such as, 1.9 eV bandgap in Au-doped C_3N_4 with slight enhancement in visible light absorption. Correspondingly, doping of Ag leading to enhanced charge separation and improvement in photocatalytic activity [30].

Further than bandgap narrowing and increased charge-transfer properties, the significant increase in hyperpolarizability saw in coinage-metal-doped C_3N_4 systems is mostly credited to the high electronic coupling between the dopant atoms and the π-conjugated C_3N_4 surface. This interaction leads localized states inside the band structure and assists efficient intramolecular charge transfer, both of which contribute to enhanced NLO behavior [31-34].

While most earlier studies have examined systems with a single dopant atom and limited structural variation. Our investigation thoroughly evaluates various doping levels (2–4 atoms) designed for Cu, Ag, and Au. This methodology offers further precise regulator over the electronic characteristics and results in a broader variety of tunable NLO responses. As far as we understand it, no earlier theoretical study has accompanied a comparative DFT-based study of this type across all three coinage metals, emphasizing the novelty and potential scientific relevance of our findings.

To create unique doped complexes, pure **C_3N_4** was doped with the coinage metals copper (Cu), silver (Ag), and gold (Au). Three new series of compounds containing different numbers of Cu, Ag, and Au atoms were generated using a doping technique. Model surfaces for the Cu series include C_3N_4 doped with two Cu atoms (**C_3N_4@2Cu**), three Cu atoms (**C_3N_4@3Cu**), and four Cu atoms (**C_3N_4@4Cu**). Similarly, model surfaces for the Ag series include C_3N_4 doped with two Ag atoms (**C_3N_4@2Ag**), C_3N_4 doped with three Ag atoms (**C_3N_4@3Ag**), and C_3N_4 doped with four Ag atoms (**C_3N_4@4Ag**). Model surfaces for the Au series include C_3N_4 that has been doped with two Au atoms (**C_3N_4@2Au**), C_3N_4 that has been doped with three Au atoms (**C_3N_4@3Au**), and C_3N_4 that has been doped with four Au atoms (**C_3N_4@4Au**). The effects of coinage metal (Cu, Au, Ag) doping on the NLO properties of C_3N_4 has been examined in this research study via DFT simulations. All of these complexes have been investigated to better understand their electrical and optical characteristics. Our findings will help developers create metal-doped C_3N_4 materials with customized NLO characteristics for certain applications.

Computational Methodology

The computational methodology employed in this study follows well-established protocols commonly used in density functional theory (DFT)-based investigations of material systems. All calculations were performed using the Gaussian 09 software package [35]**.** Molecular geometries of pristine C_3N_4 and all newly designed doped complexes were optimized using the B3LYP functional in combination with the LANL2DZ basis set, which is widely accepted and has been previously validated for C_3N_4 systems in the literature [36, 37]. To ensure the reliability of the optimized geometries, frequency calculations were conducted to confirm that the structures correspond to true minima, indicated by the absence of imaginary frequencies.

Post-processing and visualization of molecular geometries and frontier orbitals were carried out using GaussView 6.0.16 [38]. Multiwfn 3.7 [39] was employed for in-depth analysis of electronic transitions, partial density of states (PDOS), and non-covalent interactions (NCI), enhancing the interpretability of electronic structure data. UV-Visible absorption spectra were calculated using the TD-DFT method at the same level of theory, incorporating aqueous solvent effects (H_2O phase). Spectral data were further refined and statistically processed using Swizard [40], and final graphical representations were generated with Origin 6.0 [41], facilitating clear and effective presentation of results.

To evaluate the nonlinear optical (NLO) properties, the static mean polarizability (α_0) and mean first hyperpolarizability (β_0) were computed, serving

as reliable descriptors of NLO activity. These parameters were calculated for both pristine and doped C_3N_4 systems to assess the influence of metal doping on their optoelectronic and NLO behavior.

Results and Discussion

Spin State Stability Analysis

Doping with transition metals (Cu, Ag, and Au) has an extra multiplicity affect [42, 43]. Before proceeding to the calculations of additional characteristics, it is required to assess the transition metal doped C_3N_4 cage's most stable spin state. The results of the spin-polarized calculations on the transition metal-doped C_3N_4 complexes are shown in Table 1.

All the calculations were performed after the evaluation of highest stable spin state C_3N_4 complexes doped with transition metals (Cu, Ag, and Au) and further properties were investigated. The variations in electron number (may be odd or even) causes a considerable change in the spin stability of the doped complexes and results of these fluctuations are mentioned in Table 1. The results revealed that the triplet spin state of C_3N_4@2Cu, C_3N_4@4Cu, C_3N_4@2Ag, C_3N_4@4Ag, C_3N_4@2Au, and C_3N_4@4Au are highly stable among triplet, singlet, quintet, and sextet states while C_3N_4@3Cu, C_3N_4@3Ag, and C_3N_4@3Au possessed doublet spin state as the most stable state. The stability of all the doped complexes was assessed by the energy difference of transition metal doped conformations amongst several spin states. In C_3N_4@2Cu, C_3N_4@4Cu, C_3N_4@2Ag, C_3N_4@4Ag, C_3N_4@2Au, and C_3N_4@4Au the sextet state was found to be the minimum stable state exhibiting largest values of energy but in C_3N_4@3Cu, C_3N_4@3Ag, and C_3N_4@3Au the least stable state was octet spin state. The energy alterations of first stable state as well as spin states having subsequent stability was also calculated and given in Table 1.

The analysis reveals a strong correlation between the number of dopant atoms and the preferred spin state. Complexes with even numbers of Cu, Ag, or Au dopants (e.g., C_3N_4@2Cu, C_3N_4@4Ag) stabilize in a triplet ground state, whereas those with odd dopant counts (e.g., C_3N_4@3Cu, C_3N_4@3Au) favor a doublet configuration. These results reflect electron pairing trends and the occupation of metal-induced mid-gap states. In even-numbered systems, the triplet state minimizes exchange repulsion and maintains favorable electronic delocalization. Conversely, odd-numbered systems host a singly unpaired electron in the SOMO, stabilizing the doublet configuration.

This spin state behavior is highly significant for NLO activity. Open-shell configurations (triplet and doublet) often exhibit lower HOMO–LUMO gaps, enhanced intra- and inter-molecular charge transfer (ICT)**,** and stronger dipolar polarizability, all of which are critical for increasing the first (β) and second (γ) hyperpolarizabilities. The presence of unpaired d-electrons from the metal centers creates accessible low-lying excited states, enabling stronger nonlinear optical responses under applied electromagnetic fields. Hence, identifying the ground-state multiplicity provides both structural and electronic insight into the origin of enhanced NLO performance in these systems.

Table-1: Absolute energies (E) and Relative energies (R.E) in kcal mol-1 at different spin states of complexes.

C_3N_4@2Cu			
Stability	**States**	**E**	**R. E**
1st	**Triplet**	**-1607428.84**	**0**
2nd	**Singlet**	**-1607412.05**	**-16.79**
3rd	**Quintet**	**-1607397.93**	**-30.90**
4th	**Sextet**	**-1607330.23**	**-98.60**
C_3N_4@3Cu			
Stability	**States**	**E**	**R. E**
1st	**Doublet**	**-1730561.08**	**0**
2nd	**Quintet**	**-1730560.50**	**-0.56**
3rd	**Sextet**	**-1730469.45**	**-91.63**
4th	**Octet**	**-1730407.61**	**-153.47**
C_3N_4@4Cu			
Stability	**States**	**E**	**R. E**
1st	**Triplet**	**-1853653.59**	**0**
2nd	**Singlet**	**-1853630.52**	**-23.07**
3rd	**Quintet**	**-1853601.27**	**-52.33**
4th	**Sextet**	**-1853539.88**	**-113.71**
C_3N_4@2Ag			
Stability	**States**	**E**	**R. E**
1st	**Triplet**	**-1544194.40**	**0**
2nd	**Singlet**	**-1544184.79**	**-9.611**
3rd	**Quintet**	**-1544129.57**	**-64.83**
4th	**Sextet**	**-1544060.25**	**-134.15**
C_3N_4@3Ag			
Stability	**States**	**E**	**R. E**
1st	**Doublet**	**-1635701.52**	**0**
2nd	**Quintet**	**-1635653.22**	**-48.30**
3rd	**Sextet**	**-1635595.69**	**-105.83**
4th	**Octet**	**-1635531.06**	**-170.46**
C_3N_4@4Ag			
Stability	**States**	**E**	**R. E**
1st	**Triplet**	**-1727185.72**	**0**
2nd	**Singlet**	**-1727185.43**	**-0.29**
3rd	**Quintet**	**-1727134.87**	**-50.85**
4th	**Sextet**	**-1727064.55**	**-121.17**
C_3N_4@2Au			
Stability	**States**	**E**	**R. E**
1st	**Triplet**	**-1531260.97**	**0**
2nd	**Singlet**	**-1531223.52**	**-37.4472006**
3rd	**Quintet**	**-1531180.37**	**-80.60**
4th	**Sextet**	**-1531114.39**	**-146.57**
C_3N_4@3Au			
Stability	**States**	**E**	**R. E**
1st	**Doublet**	**-1616270.31**	**0**
2nd	**Quintet**	**-1616228.26**	**-42.04**
3rd	**Sextet**	**-1616182.13**	**-88.17**
4th	**Octet**	**-1616117.09**	**-153.22**
C_3N_4@4Au			
Stability	**States**	**E**	**R. E**
1st	**Triplet**	**-1701310.81**	**0**
2nd	**Singlet**	**-1701296.69**	**-14.12**
3rd	**Quintet**	**-1701228.38**	**-82.43**
4th	**Sextet**	**-1701190.42**	**-120.39**

Geometry Optimization and Thermodynamic Stability

The optoelectronic and structural characteristics are profoundly influenced by geometry optimization [44]. By applying DFT/LANL2DZ to optimize the reference surface C_3N_4 and all the new doped complexes, the examined systems' structures were stabilized by shifting them to their respective energy minima. Fig. 1 shows the optimized frameworks of the ideal structures for C_3N_4 and all the doped complexes.

Eq. 1 [45] was applied to evaluate vertical ionization energy (VIE) (see Table 2).

$$\boldsymbol{VIE = -E_{HOMO}\,(g_N)} \qquad \textbf{(1)}$$

The energy of the highest occupied molecular orbital (HOMO) of the N-electron system is represented here by the $-E_{HOMO}\,(g_N)$.

In order to test the thermodynamic stability, vertical ionization energies (VIE) were applied. According to Table 2, all investigated compounds exhibited VIE values that were between 3.86 and 5.52 eV less than those of pure C_3N_4, indicating that all newly doped complexes are more stable than pure C_3N_4. As compared to other freshly doped complexes, C_3N_4@3Au is the most thermodynamically stable and has a higher value of VIE (Fig. 2).

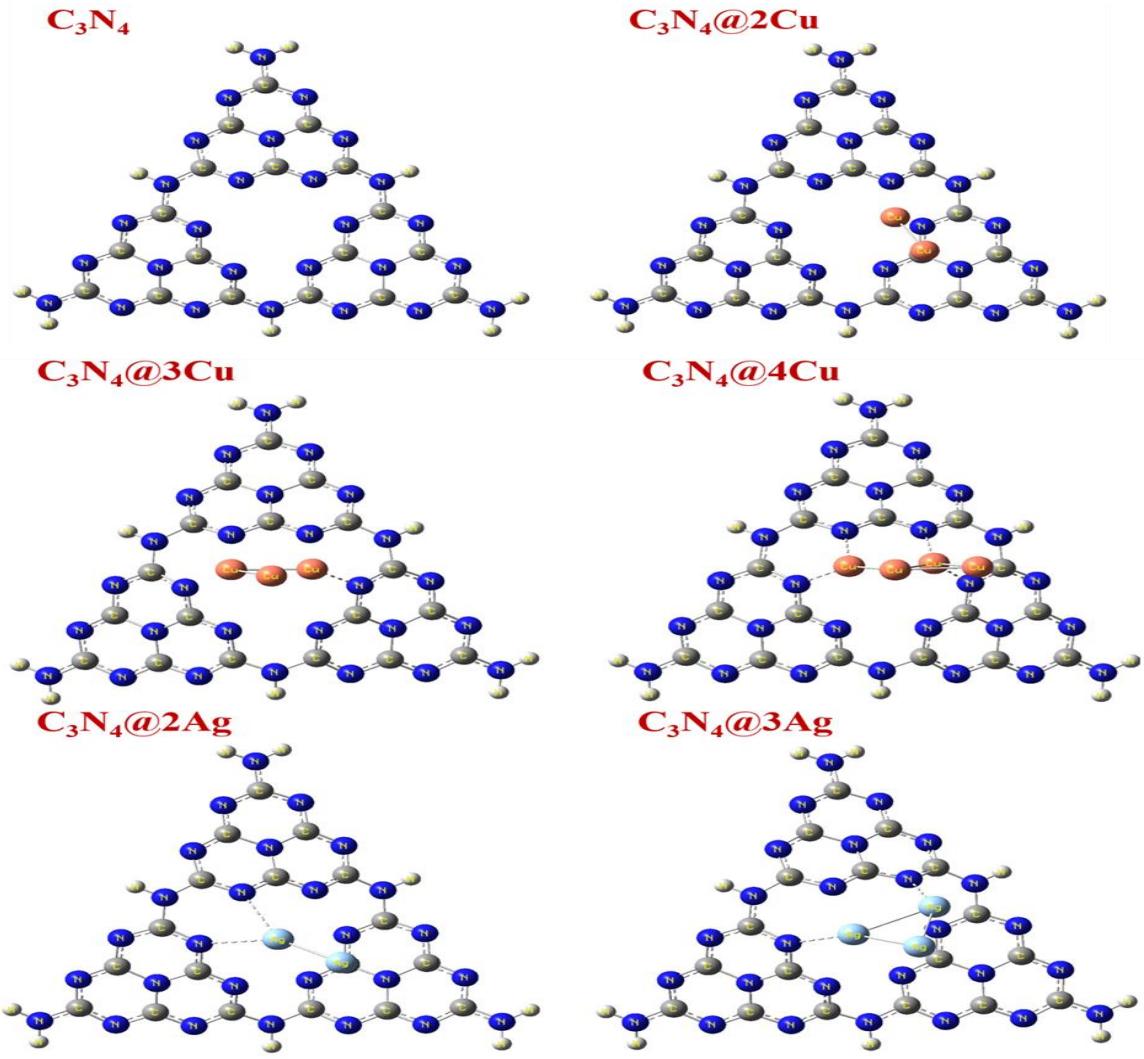

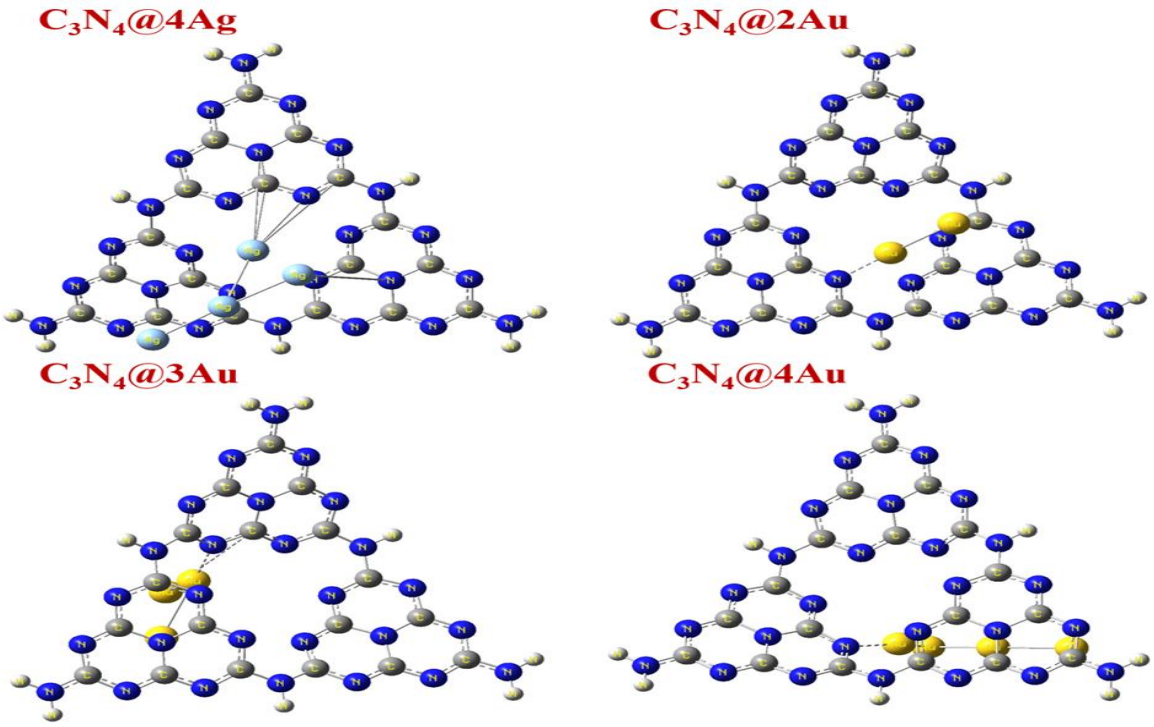

Fig. 1: Optimized molecular geometries of pristine C_3N_4 and the metal-doped C_3N_4 complexes obtained at the B3LYP/LANL2DZ level of theory.

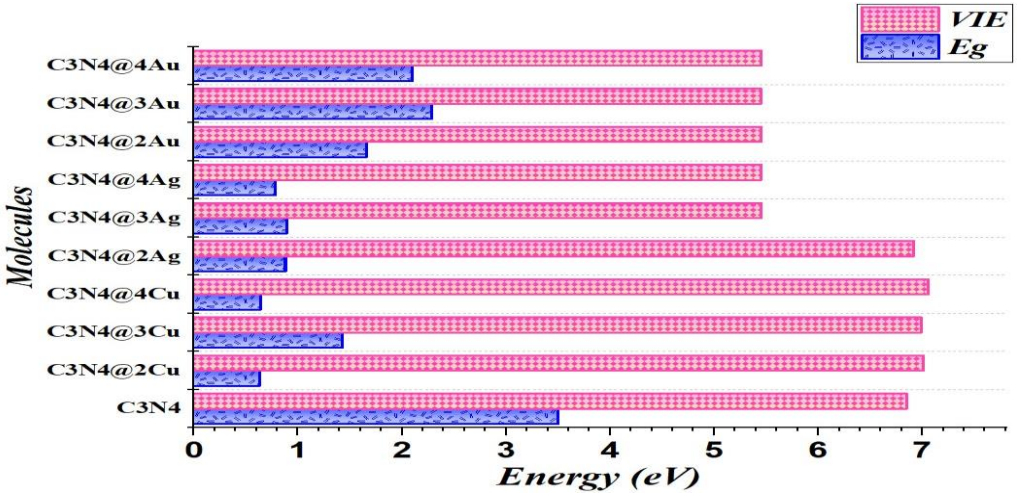

Fig. 2: Comparison bar chart of bandgap (E_g) and vertical ionization energy (VIE) of researched structures.

Table-2: Computed values of EH, EL, Eg, S, η, and EVI for the investigated structures.

Compounds	E_H (eV)	E_L (eV)	E_g (eV)	*S* (eV)	η (eV)	E_{VI} (eV)
C_3N_4	-6.39	-2.89	3.50	0.57	1.75	6.39
C_3N_4@2Cu	-3.89	-3.26	0.63	3.13	0.32	3.89
C_3N_4@3Cu	-4.52	-3.09	1.43	1.39	0.72	4.52
C_3N_4@4Cu	-3.86	-3.22	0.64	3.13	0.32	3.86
C_3N_4@2Ag	-4.12	-3.24	0.88	2.27	0.44	4.12
C_3N_4@3Ag	-3.93	-3.04	0.89	2.22	0.45	3.93
C_3N_4@4Ag	-4.10	-3.32	0.78	2.56	0.39	4.10
C_3N_4@2Au	-5.01	-3.35	1.66	1.20	0.83	5.01
C_3N_4@3Au	-5.52	-3.23	2.29	0.87	1.15	5.52
C_3N_4@4Au	-5.51	-3.41	2.10	0.95	1.05	5.51

FMO Analysis, Kinetic Stability, and Chemical Reactivity

Effective knowledge of optical and conduction characteristics is provided by frontier molecular orbital (FMO) study. To do this, FMO calculations were carried out using the chosen DFT technique, LANL2DZ, and GaussView was used to create the visual representation as shown in Fig. 3. The band gap (E_g) between these orbitals, which was estimated using Eq. 2, [46] is also included in the FMO research.

$$E_g = E_L - E_H \quad (2)$$

Here, E_L and E_H are energies of LUMO and HOMO, respectively.

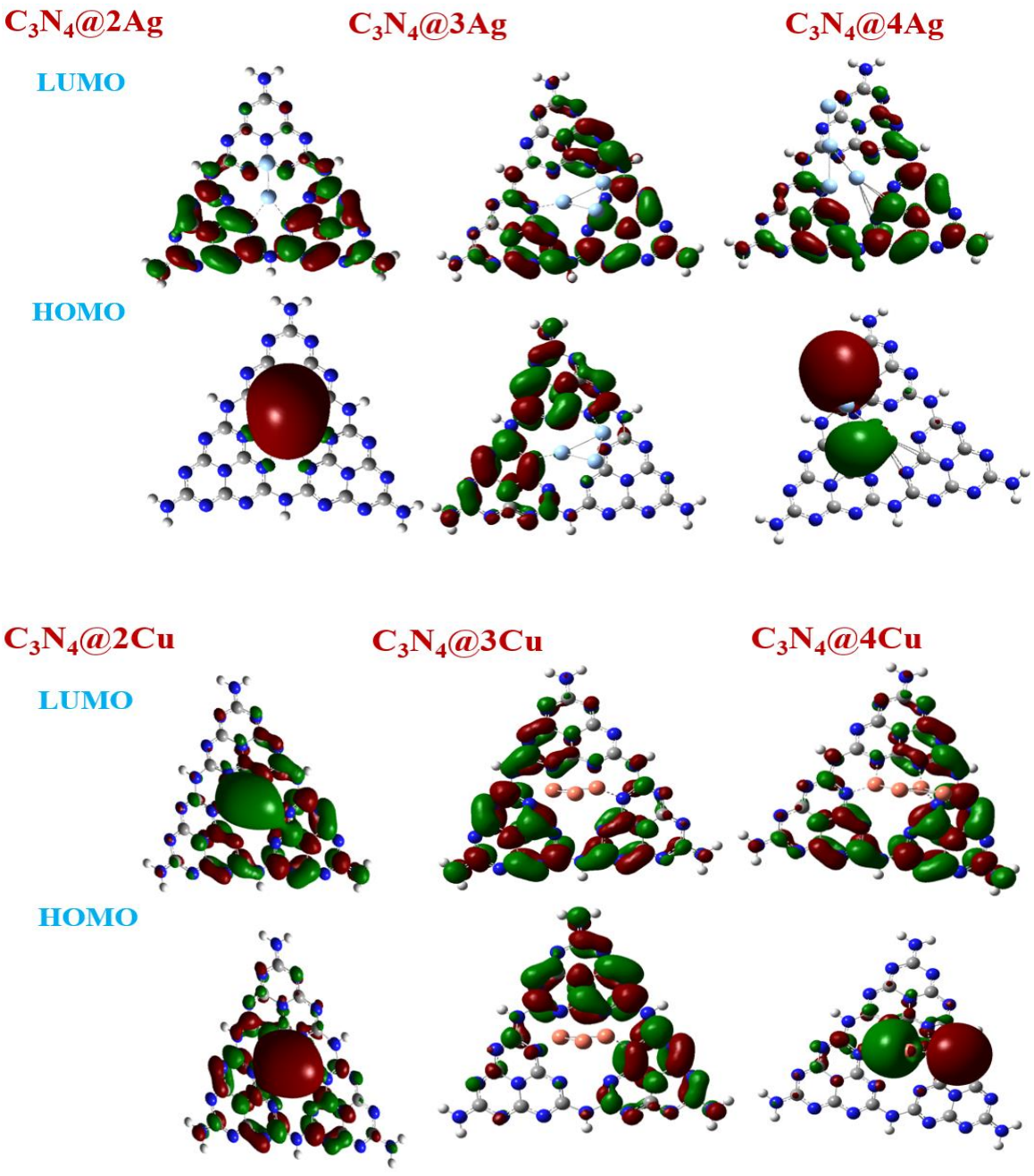

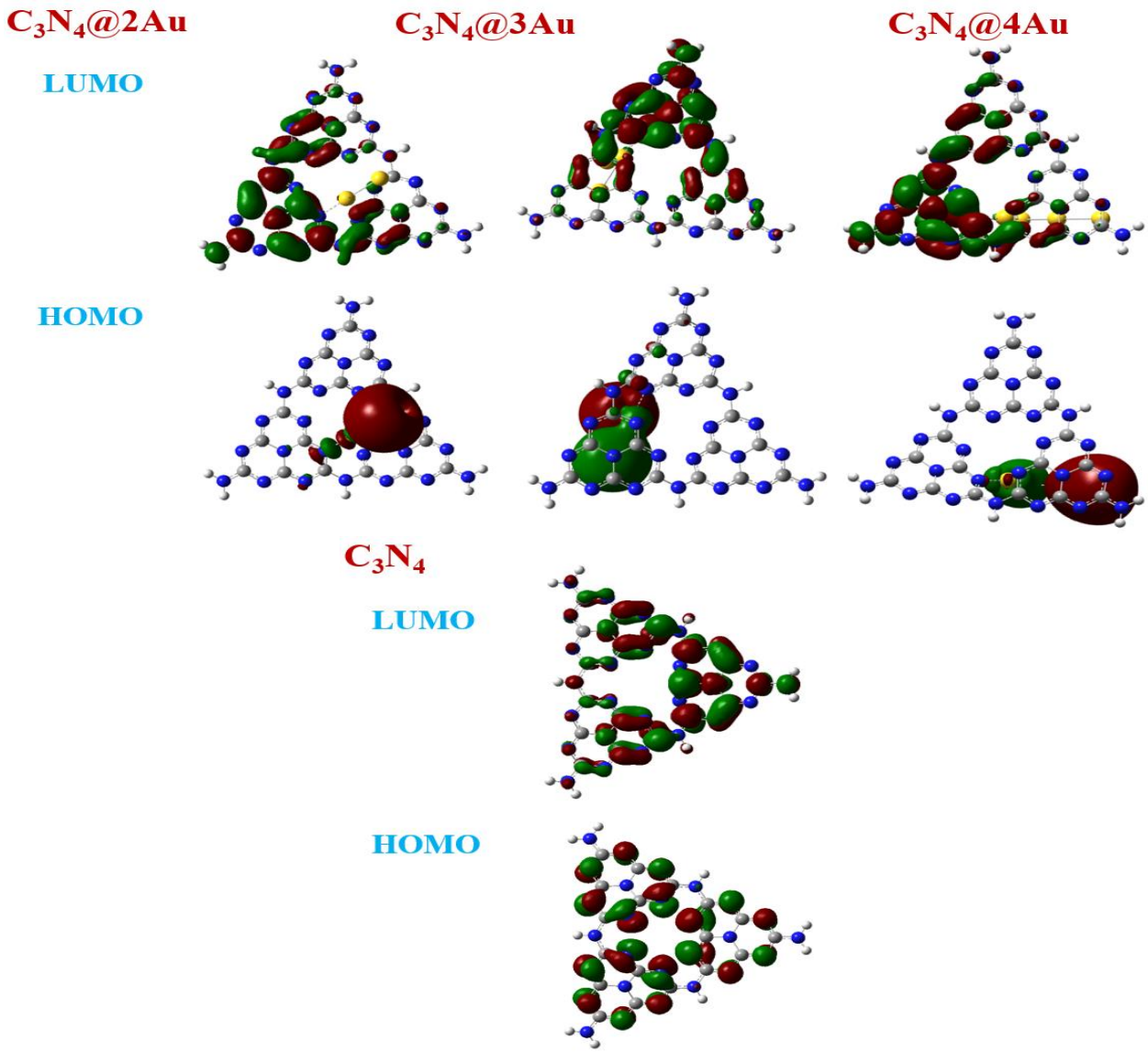

Fig. 3: Graphical depiction of HOMO and LUMO orbitals in the optimized structures.

Table 2 lists the HOMO and LUMO energies, band gap, and new doped complexes. The findings showed that the HOMO and LUMO energies of model C_3N_4 are -6.39 and 2.89 eV, respectively, with an energy gap of 3.50 eV. Nevertheless, following the doping of transition metal atoms, a significant reduction in bandgap was seen. The results make it clear that adding more transition metal atoms to a pure surface causes the band gap to close, leading to enhanced charge transfer. Band gap and charge transfer are inversely correlated. Excellent optical and electrical characteristics are possessed by the high charge transfer value.

The pictorial representation of FMO describes the HOMO and LUMO charge densities present on the molecule. The model C_3N_4 surface has its HOMO orbitals more condensed on central cavity while LUMOs are present on peripheral part of the surface and band gap is high. But after the doping of surface with varying number of transition metal (Cu, Ag, Au) the charge density of HOMOs as well as LUMOs was shifted to different parts thereby increasing charge transfer and contracting band gap. In C_3N_4@3Cu and C_3N_4@3Ag the HOMO as well as LUMO electronic density is populated on varying portion of C_3N_4 surface merely. In all doped complexes except C_3N_4@3Cu and C_3N_4@3Ag, the FMO distribution pattern is alike, the HOMO density

is concentrated on transition metal atoms acting as electron donor while LUMO density is present of surface acting as electron acceptor there by decreasing band gap and enhancing charge transfer that is favorable for efficient optoelectronic materials.

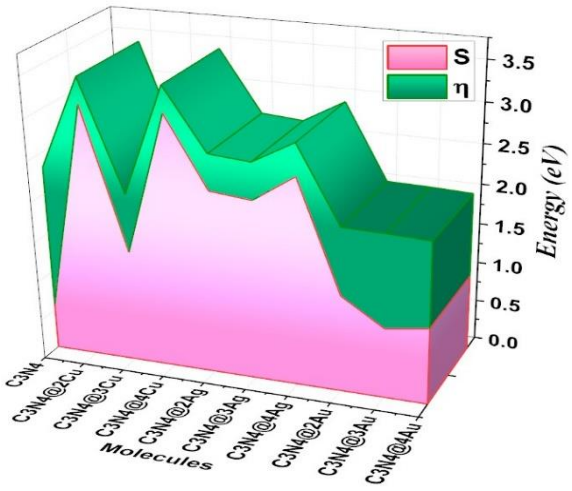

Fig. 4: Graphical representation of softness (S) and chemical hardness (η) for the investigated structures.

$$Chemical\ hardness\ (\eta) = \frac{(E_{LUMO} - E_{HOMO})}{2} \quad (3)$$

$$Chemical\ softness\ (S) = \frac{1}{\eta} \quad (4)$$

Chemical hardness (η) by Eq. 3 and chemical softness (S) using Eq. 4 have been simulated [47] and shown in Fig. 4. Low chemical hardness measurements represent the degree of polarization (soft nature) as displayed in Table 2.

A soft molecule is one that has a narrow bandgap and is highly polarizable, poor in kinetic stability, and high in chemical reactivity [48]. Based on low E_g, it is claimed that all modelled doped systems are effective charge transfer materials that are reactive as well as polarizable. eV HOMO and LUMO values in Fig. 5(a) and E_g, are graphically shown in Fig. 5(b).

Dipole Moment

A crucial factor in determining the crystal quality and atom packing in a structure is the dipole moment of molecules. The result of distance and charge determines a molecule's polarity [49, 50]. Increased polarity indicates enhanced crystal structure and stable molecular packing. The larger dipole moment also stands for the molecular structure's decreased flaws and calming anomalies. The reserved symmetry is what causes the low value of the dipole moment, whereas a change in symmetry results in an increase in the dipole moment and an increase in polarization, which is advantageous for improving charge transfer and enhancing optoelectronic capabilities.

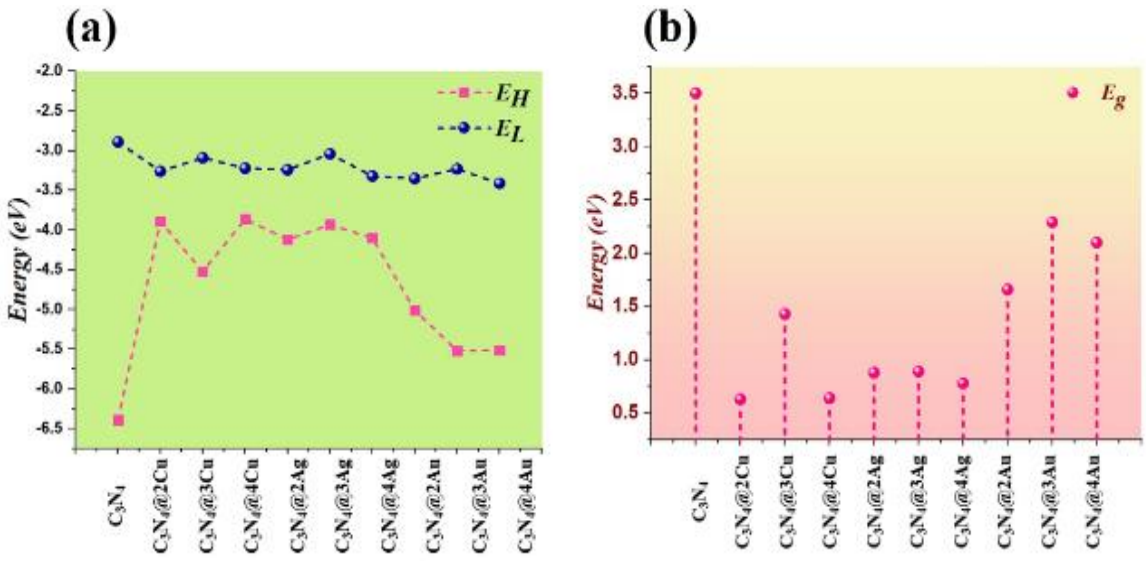

Fig. 5: HOMO, LUMO energies (a) and bandgap (b) of researched structures.

Two different forms of dipole moments were computed for surface C_3N_4 and all new complexes in this investigation at the same theoretical level, and the findings are shown in Table **3**. The excited state dipole moment (μ_e) is higher than the ground state dipole moment (μ_g) advocating the fact that newly proposed complexes are miscible in H_2O. On a pure C_3N_4 surface, the μ_g is equal to 1.4643 D and μ_e is equal to 2.2343 D however following the addition of Cu, Ag, and Au atoms, the values of the dipole moment rose. The findings showed that the value of the dipole moment grew in both phases along with the number of doped atoms, reaching its maximum for C_3N_4@4Au, where four Au atoms are doped in the surface C_3N_4.

Table 3. Computed transition dipole moment (Delta μ), ground-state dipole moment (μ_g), and excited-state dipole moment (μ_e) for the investigated structures.

Compounds	Δμ (au)	μ_g (D)	μ_e (D)
C_3N_4	0.5104	1.4643	2.2343
C_3N_4@2Cu	2.2656	2.2929	8.1646
C_3N_4@3Cu	3.8145	3.3311	6.6757
C_3N_4@4Cu	1.9766	1.2851	6.4097
C_3N_4@2Ag	0.5899	6.3553	7.0218
C_3N_4@3Ag	1.4201	3.1500	6.3259
C_3N_4@4Ag	1.5734	8.0073	10.5407
C_3N_4@2Au	0.6790	4.9267	4.3823
C_3N_4@3Au	1.1437	5.1558	9.4393
C_3N_4@4Au	1.1337	10.1257	12.5659

Another parameter, transition dipole moment (Δμ) was also calculated from ground state to excited state for all the studied systems. The value of transition dipole moment for model surface C_3N_4 is 0.5104 au while increase in its value is observed after doping as presented in Table 3. The results of dipole moment might be suiTable for optoelectronic applications of the designed materials.

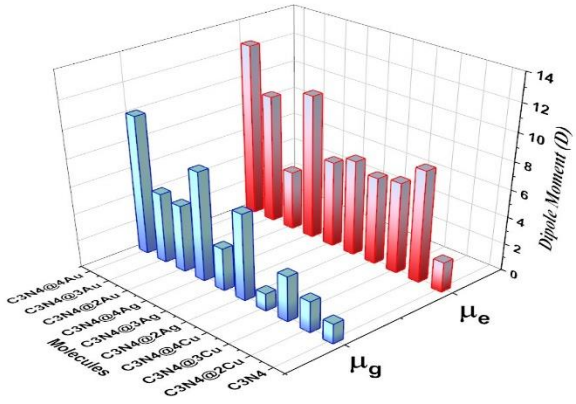

Fig. 6: Graphical depiction of dipole moment of researched structures.

UV-Visible Absorption

With the aid of the LANL2DZ level of theory, UV-Visible absorption analysis utilizing the TD-DFT technique was carried out to explore the photophysical and optoelectronic characteristics of C_3N_4 and all doped systems in the solvent phase of water [51]. Using Origin software, the λ_{max} was plotted in graphical form and shown in Fig. 7. The λ_{max} of the undoped model C_3N_4 was 383 nm, which is very low, however the resultant molecules displayed improved absorption in the visible and near infrared area following Cu, Ag, Au doping.

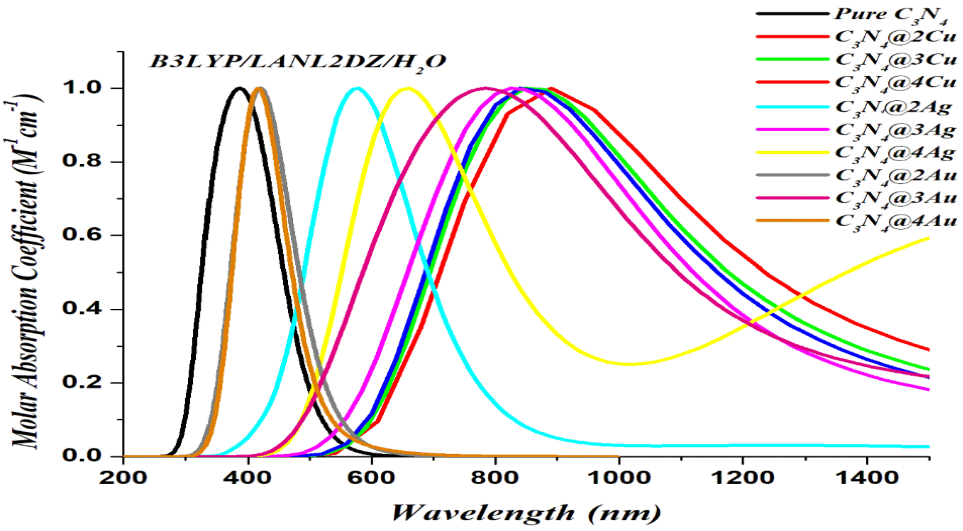

Fig. 7: UV-vis spectra of researched structures.

All of the systems under study were transparent to UV light, but following doping, all complexes displayed substantial absorption. **C_3N_4@2Cu** demonstrated the greatest absorption. As **C_3N_4@2Cu** had the lowest band gap and the largest absorption, it increased charge transfer and electronic excitation by absorbing at longer wavelengths. This increase in absorption is also connected to low band gap. Due to low band gap transitions, the bathochromic shift (absorption shifting to longer wavelengths) seen in doped complexes is the result of π to π*. Table 4 lists the λ_{max} as well as other photophysical characteristics.

The bathochromic shifts observed in the UV-Visible absorption spectra of the doped C_3N_4 systems, particularly C_3N_4@2Cu, suggest a strong potential for improving the performance of optoelectronic devices. The extension of absorption into the visible and near-infrared regions enables more efficient harvesting of solar photons, which is crucial for enhancing photo response in applications such as solar energy conversion and photocatalysis. The reduction in the band gap and the associated redshift in λ_max facilitate more effective π→π* electronic transitions, leading to improved charge excitation and separation under illumination. These modifications directly impact the optoelectronic efficiency by increasing the light absorption range and reducing energy losses. Therefore, the enhanced optical response of the doped systems highlights their practical relevance for use in visible-light-active photocatalysts, photodetectors, and other light-driven technologies.

Excitation energy (ΔE), a crucial quantity that determines how quickly electrons move from HOMO to LUMO when light in the visible or near-infrared spectrum is absorbed, was also estimated. Undoped C_3N_4 has ΔE of 3.23 eV, although doping causes a significant drop in ΔE. C_3N_4@2Cu, which likewise exhibits the highest electron transfer and greatest absorption, has the lowest value. Because lower the ΔE higher will be the absorption as well as ICT that results in efficient optoelectronic materials.

Oscillator strength (f_{osc}) is another important dimensionless quantity that indicates the likelihood that electrons would absorb radiation during transitions from HOMO to LUMO. f_{osc} values are listed in Table 4 and Fig. 8 displays its trend.

Table-4: UV-Visible absorption profiles of the studied compounds in aqueous phase.

Compounds	λ_{max} (nm)	ΔE (eV)	f_{osc}	LHE	% C. I	Transition
C_3N_4	383	3.23	0.01	0.02	64	H→ L
C_3N_4@2Cu	886	1.39	0.10	0.21	72	H→ L
C_3N_4@3Cu	854	1.45	0.23	0.41	83	H→ L
C_3N_4@4Cu	842	1.47	0.21	0.38	80	H→ L
C_3N_4@2Ag	594	2.09	0.02	0.05	83	H→ L
C_3N_4@3Ag	856	1.45	0.23	0.41	82	H→ L
C_3N_4@4Ag	650	1.91	0.01	0.02	84	H→ L
C_3N_4@2Au	438	2.83	0.01	0.02	74	H→ L
C_3N_4@3Au	792	1.57	0.01	0.02	86	H→ L
C_3N_4@4Au	415	2.99	0.17	0.32	85	H→ L

The Table 4 lists the main electron transitions from the ground state HOMO to the excited state LUMO, along with their percentage contributions, which range from 60 to 90%.

A method for calculating the effectiveness of light harvesting is also necessary for evaluating the compounds' optical value. The oscillatory strength (f_{osc}) value governs light harvesting efficiency (LHE), which is a reflection of the compound photocurrent response [52].

$$LHE = 1 - 10^{-fosc} \quad (5)$$

Significant LHE values are present in compounds with strong photocurrent responses, and vice versa. Table 4 provides the LHE in solvent phase for all chemicals using equation [53] while its trend compared with excitation energy is shown in Fig. 9**.** Newly developed compounds have been shown to have dramatically different LHE values as a result of structural changes, which may be related to the increased photocurrent output of these structures.

DOS Analysis

FMOs study of all investigated compounds has been supported by Mullikan's charge in current research project. DOS analysis has improved our understanding of each molecule fragment's involvement in electronic excitation and absorption at HOMO-LUMO [54]. Graphical view of DOS analysis in displayed in Fig. 10.

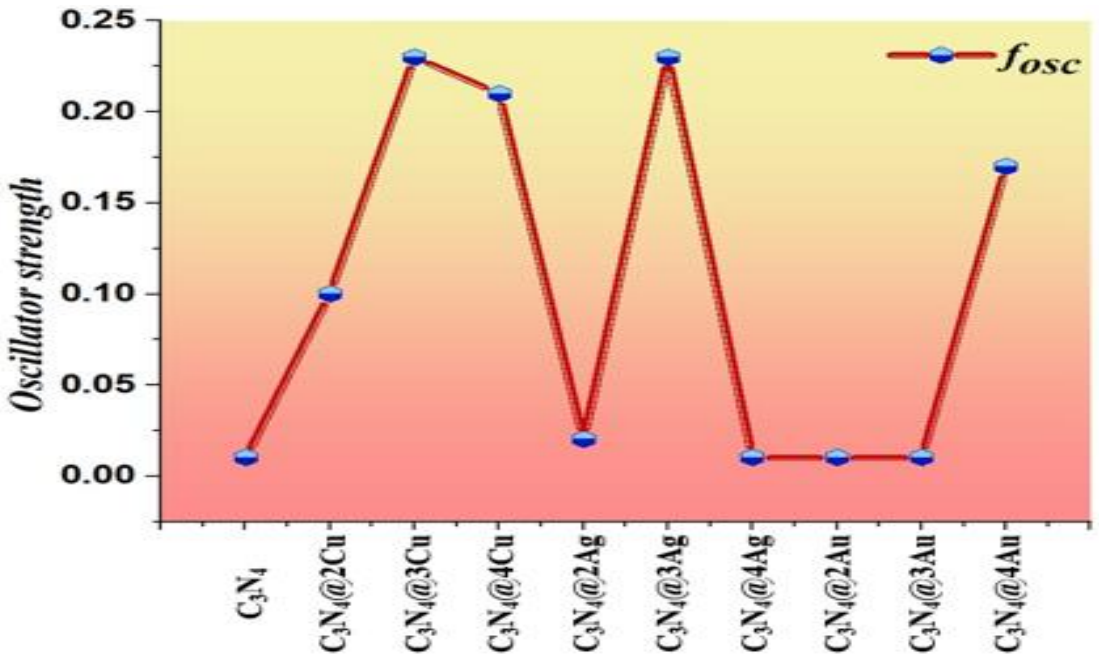

Fig. 8: Graphical depiction of oscillator strength (f_{osc}) of researched structures.

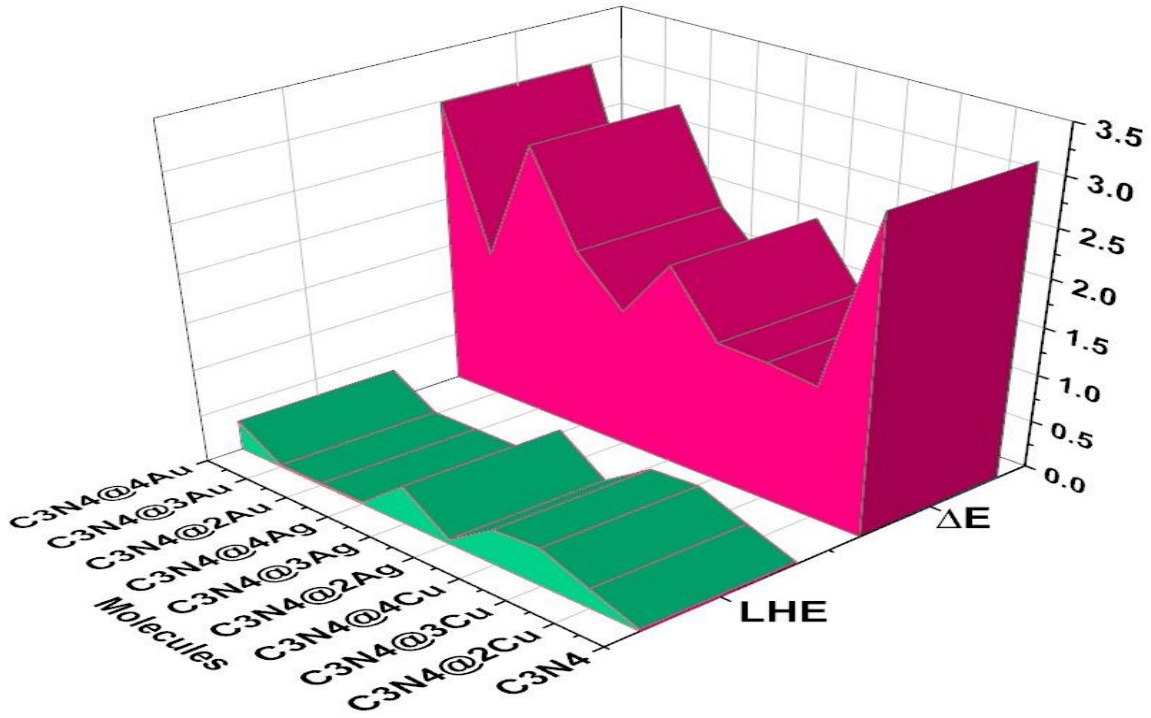

Fig. 9: Graphical depiction of excitation energy (ΔE) and light harvesting efficiency (LHE) of researched structures.

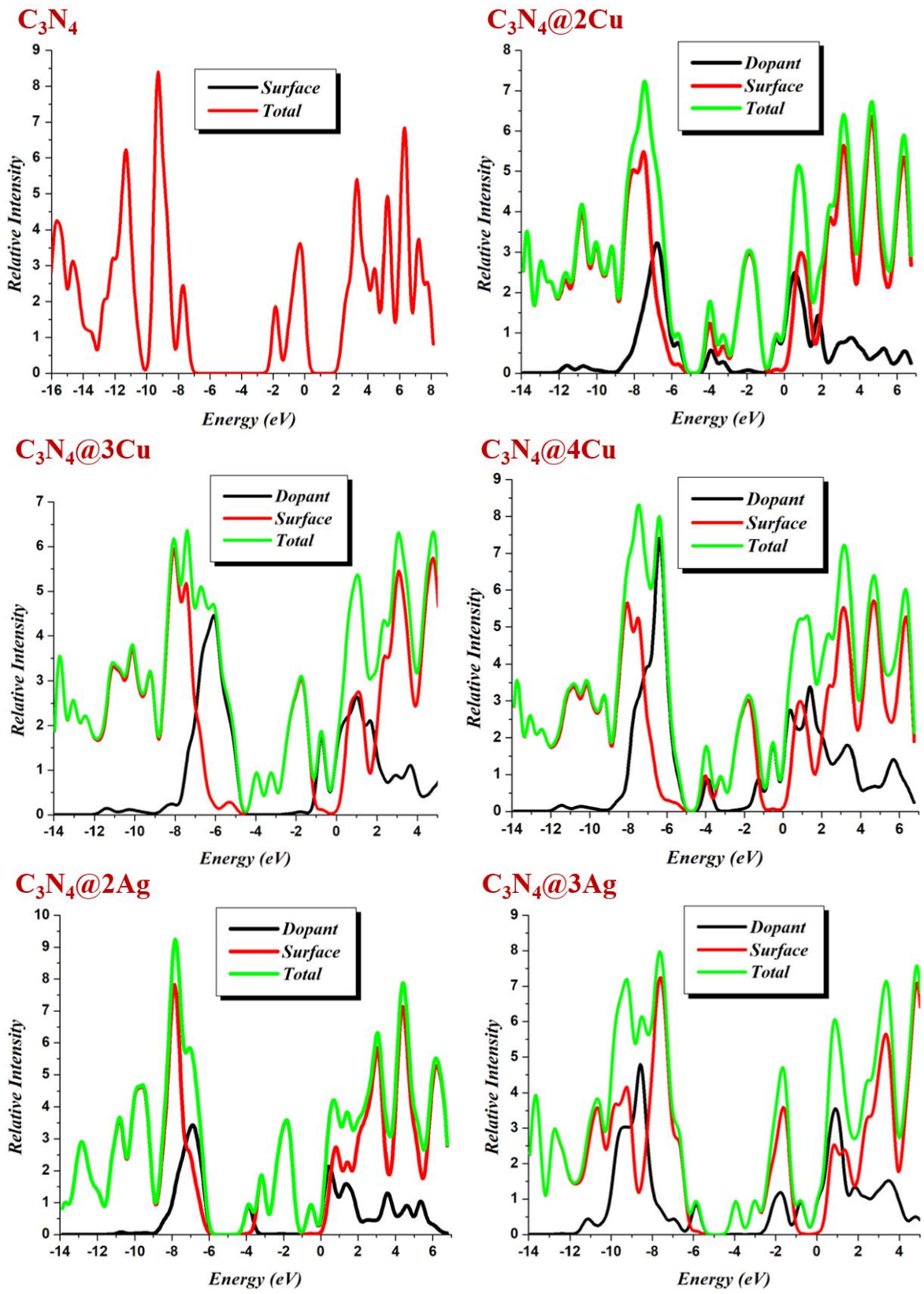
C3N4
Surface
Total
Relative Intensity
Energy (eV)
C3N4@2Cu
Dopant
Surface
Total
Relative Intensity
Energy (eV)
C3N4@3Cu
Dopant
Surface
Total
Relative Intensity
Energy (eV)
C3N4@4Cu
Dopant
Surface
Total
Relative Intensity
Energy (eV)
C3N4@2Ag
Dopant
Surface
Total
Relative Intensity
Energy (eV)
C3N4@3Ag
Dopant
Surface
Total
Relative Intensity
Energy (eV)

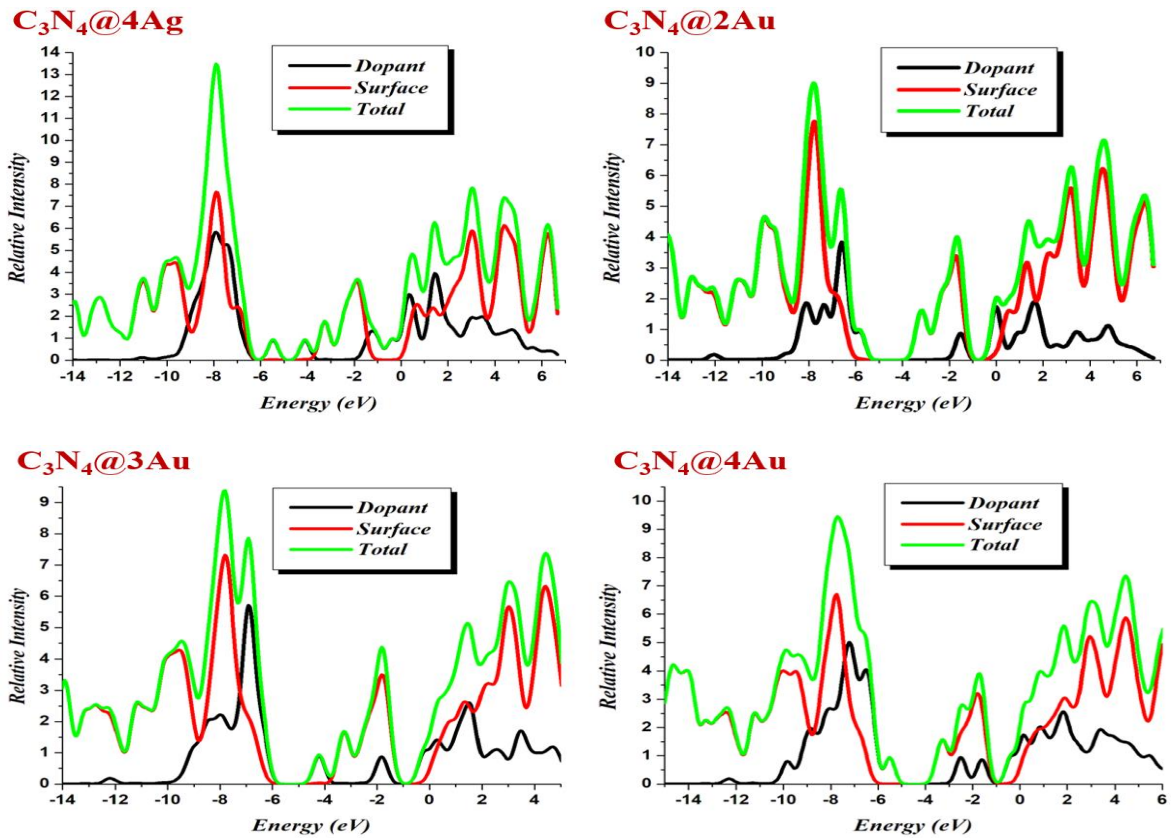

Fig. 10: DOS graphs of researched structures.

Here, the TDOS (Total Density of State) is shown by the green line, while the PDOS (Partial Density of State) is distinguished by the colour lines that are red (for the surface) and black (for the dopant).

Table-5: Electronic Density of States profiles for the studied compounds.

Compounds	HOMO = H LUMO = L	Surface	Dopant
C_3N_4	H	100	—
	L	100	—
C_3N_4@2Cu	H	47.3	52.7
	L	70.6	29.4
C_3N_4@3Cu	H	99.5	0.5
	L	99.7	0.3
C_3N_4@4Cu	H	12.1	87.9
	L	99.5	0.5
C_3N_4@2Ag	H	3.2	96.8
	L	99.7	0.3
C_3N_4@3Ag	H	99.4	0.6
	L	99.5	0.5
C_3N_4@4Ag	H	4.2	95.8
	L	99.3	0.7
C_3N_4@2Au	H	3.3	96.7
	L	99.5	0.5
C_3N_4@3Au	H	3.8	96.2
	L	97.3	2.7
C_3N_4@4Au	H	1.2	98.8
	L	99.2	0.8

In pristine C_3N_4, both the HOMO and LUMO levels are primarily contributed by surface atoms, indicating that charge generation and transition pathways are intrinsic to the undoped framework. However, upon metal doping, a significant reconfiguration of the DOS profile is observed. For all doped systems, the HOMO states show dominant contributions from dopant atoms (Cu, Ag, or Au), while the LUMO remains largely composed of surface atom contributions. This spatial redistribution indicates the establishment of an internal donor–acceptor system, where the dopants act as electron donors and the surface atoms function as electron acceptors.

The DOS analysis provides valuable insight into the modifications in the electronic structure induced by doping and offers a clear rationale for the enhanced optoelectronic behavior observed in these systems. The pronounced dopant contribution to the HOMO results in a reduced band gap, which correlates well with the bathochromic shifts in UV-Visible absorption spectra and increased λ_max values (Table 4). Notably, **C_3N_4@2Cu** exhibits the most significant HOMO shift toward the Fermi level, aligning with its lowest band gap and strongest absorption in the visible region. This reduction in band gap facilitates π→π* transitions at

lower energies and promotes more effective electronic excitation.

Furthermore, the separation of charge carrier localization between the HOMO and LUMO (on dopant and surface atoms, respectively) suggests improved charge separation and reduced recombination, which are critical for the performance of optoelectronic and photocatalytic devices. Thus, the DOS results not only reinforce the TD-DFT optical findings but also provide a mechanistic basis for the observed improvements in the photophysical and electronic properties of the doped C_3N_4 systems.

NCI Analysis

Using NCI plots and the Multiwfn software, important details on weak forces of interactions, or non-covalent interactions, between atoms in the complex system has been examined. Strong forces of attraction are shown by the area of the graph with an electron density < 0, while strong forces of repulsion are indicated by the area with an electron density of > 0. The van der Waals forces of interactions are also characterized by the points in the area 0.

The NCI graphs of surface C_3N_4 and all the doped complexes have been shown in Fig. 11. Surface C_3N_4 has a few places in the zone $\lambda 2\ (\rho) < 0$, indicating no H-bonding but some Van der Waals interactions and steric hindrance. Furthermore, in all other doped systems, there are substantial concentrations zone sign $\lambda 2\ (\rho) < 0$ and $\lambda 2\ (\rho) = 0$, indicating strong attractive forces and van der Waals. This is favorable for encouraging photoelectric performance.

The colors in the NCI graphs helps to recognize the different types of non-covalent interactions. Blue regions point to resilient attractive forces, corresponding hydrogen bonding. Green areas represent weak, stabilizing interactions—mostly van der Waals forces. alternatively, red areas represent regions where atoms are too close, leading to steric clashes or repulsion. Composed, these colors provide a well-defined illustration of where the system is stabilized or stressed.

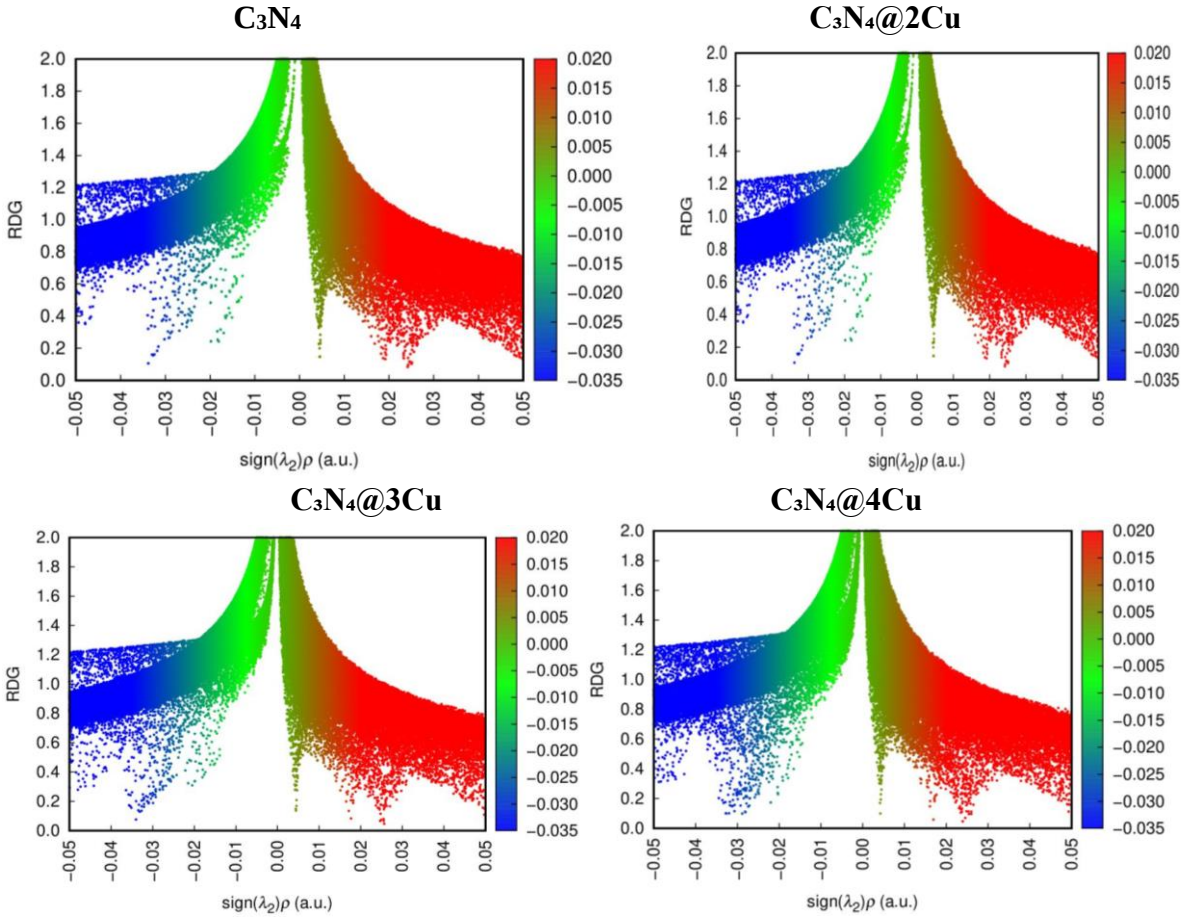

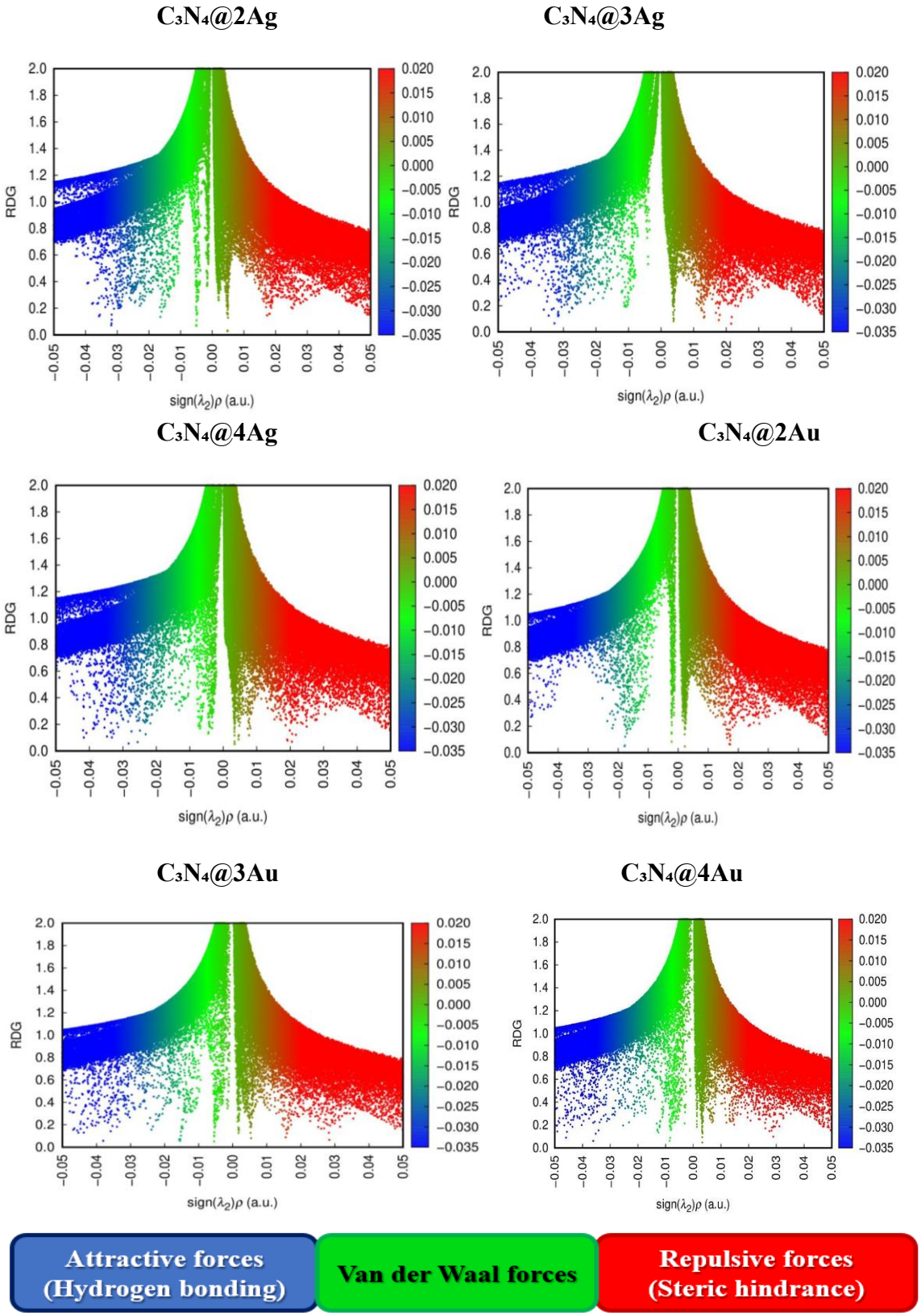

Fig. 11: NCI graphs of researched structures.

Transition Density Matrix (TDM) analysis

The strength of electronic transitions along with electron, hole allocation has been investigated via TDM examination [55, 56]. The colored bar on graphs along the right y-axis showed electron density, with the hues blue, green, and red denoting increasing potential. The graph's intense stains are made up of several atoms with higher transition rates. The doped complexes in the current investigation have been divided into two components: the surface (S) and the dopant (D) (Fig. 12).

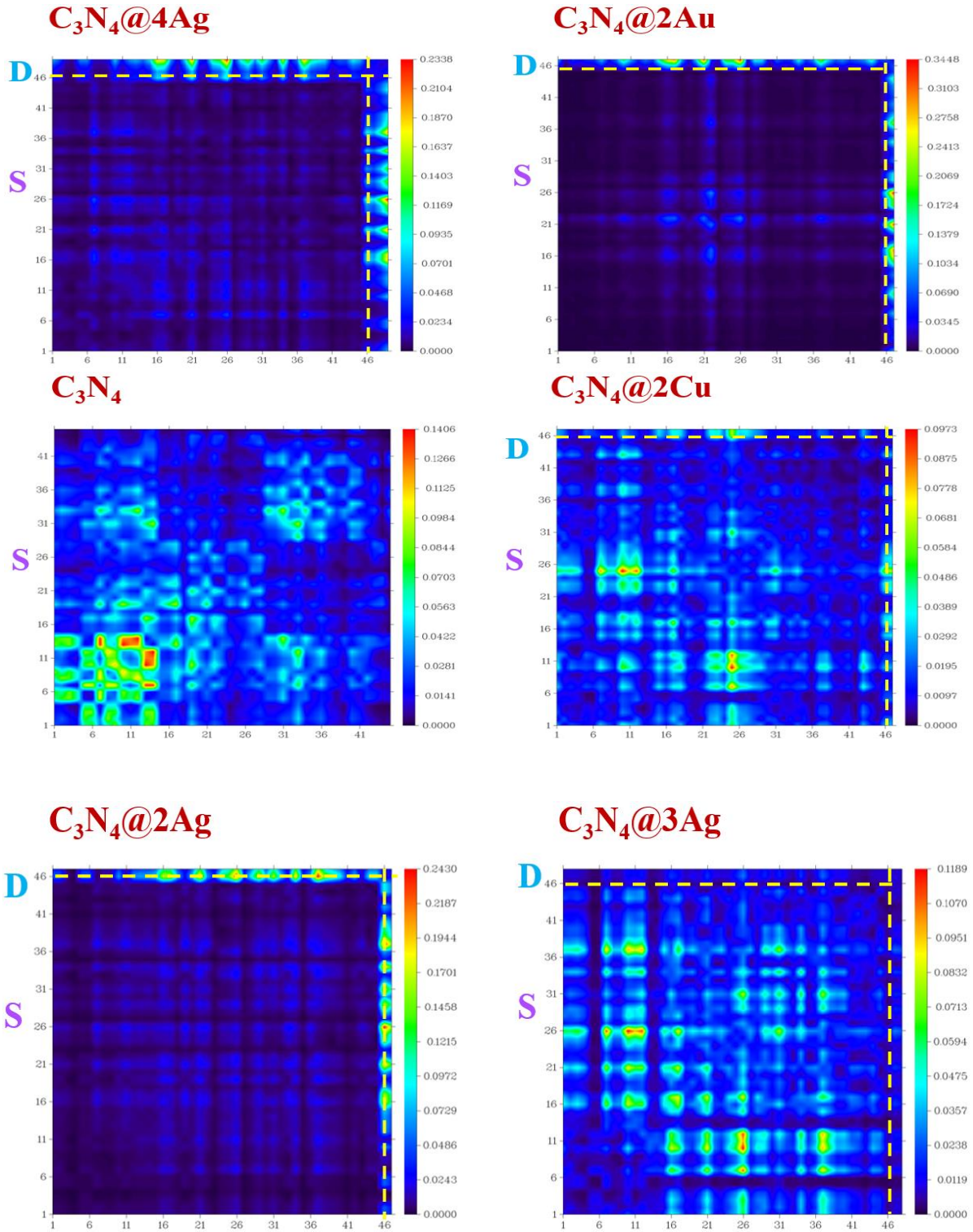

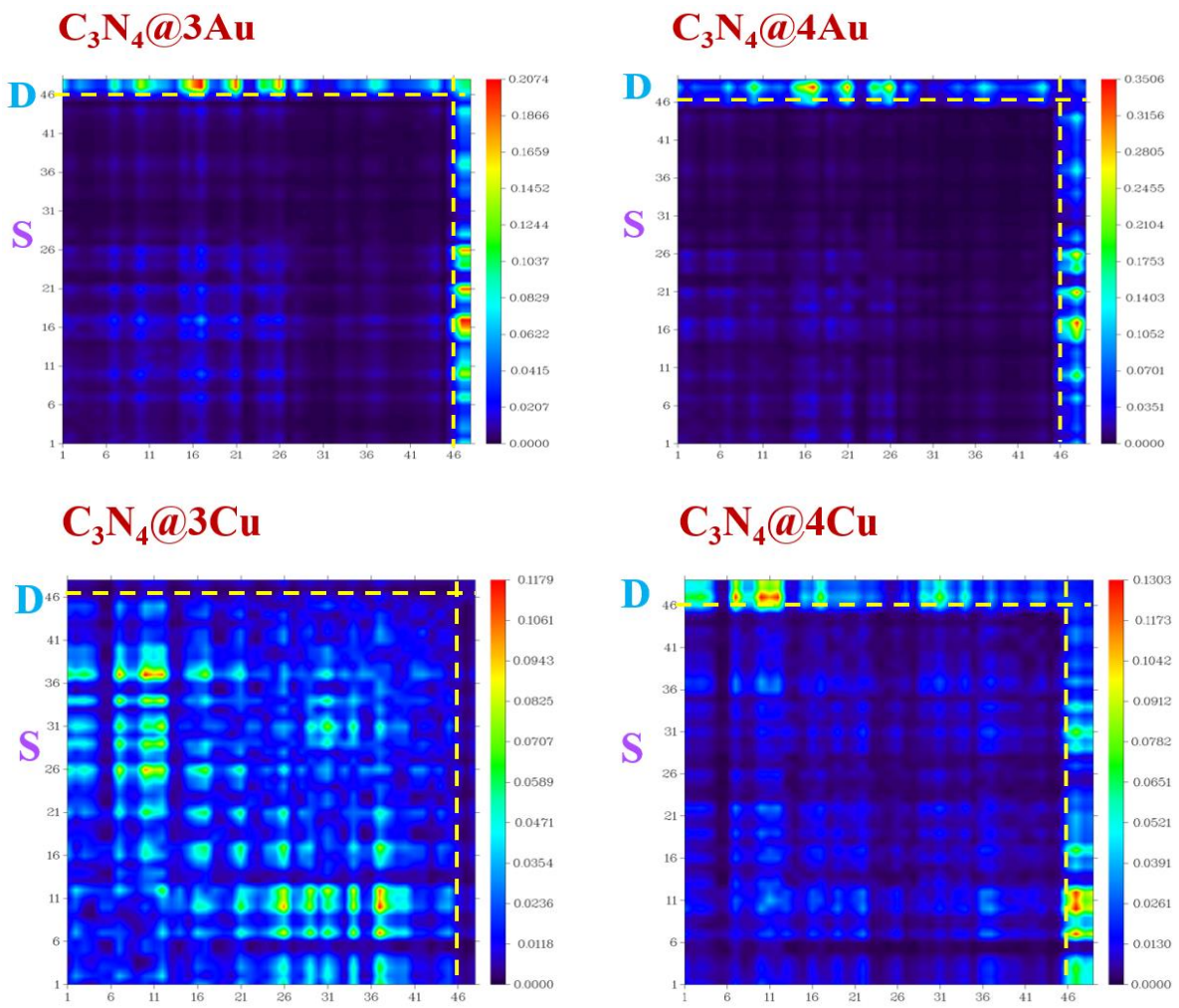

Fig. 12: TDM maps of researched structures.

In the case of pure C_3N_4, the detailed examination shows that electrons are delocalized over a broader region. Yet, the bright regions in TDM plots indicate that all newly created complexes have coherent charge distribution along with delocalization of charge. Due to effective intramolecular charge transfer, the TDM analysis also suggests that newly created compounds may be viable candidates for NLO materials.

Polarizability

When compared to the pure surface, all of the metal doped complexes showed greater isotropic (α_{iso}) and anisotropic (α_{aniso}) polarizability values as displayed in Table 6. The polarizability of the C_3N_4 surface in its purest form is 479 au, but after doping, it rises as seen in Fig. 13. Also, the comparison shows that anisotropic polarizabilities outweigh isotropic polarizabilities.

Table-6: Computed α_{iso} and α_{aniso} polarizabilities of investigated compounds.

Compounds	α_{iso} (au)	α_{aniso} (au)
C_3N_4	479.00	470.10
C_3N_4@2Cu	809.99	579.75
C_3N_4@3Cu	762.78	653.60
C_3N_4@4Cu	795.45	564.77
C_3N_4@2Ag	608.98	422.17
C_3N_4@3Ag	704.76	584.69
C_3N_4@4Ag	732.78	407.40
C_3N_4@2Au	541.81	453.32
C_3N_4@3Au	598.65	1298.65
C_3N_4@4Au	630.91	367.53

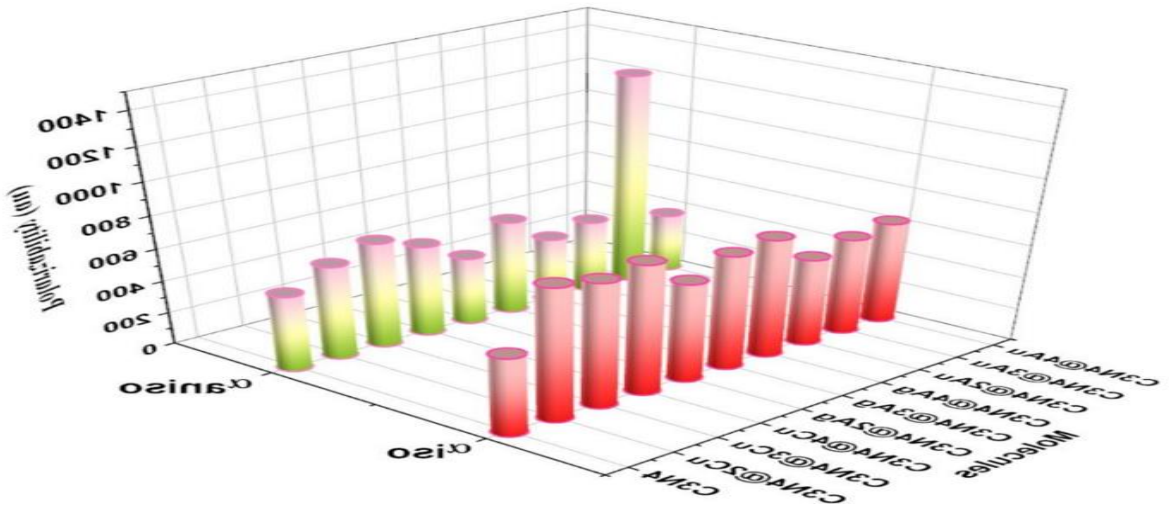

Fig. 13: Graphical illustration of α_{iso} and α_{aniso} polarizabilities of researched structures

Our findings suggested that these complexes are orientation-dependent and exhibit non-uniform behaviour in all directions. The polarized electron metal dopants are responsible for the increase in polarizabilities in all of the developed compounds. It is simple to excite these extra electrons, which lowers the transition energies and results in improved electronic characteristics. It is anticipated that all of these newly created compounds with high polarizability values would display exceptional optoelectronic and non-linear optical capabilities. The α_0 (static mean polarizability as depicted in Fig. 14, β_0 (mean first hyperpolarizability) have been computed using Eq. 6 and **7** [57,58] and results have been displayed in Fig.15.

$$\alpha_0 = \frac{1}{3}\left(\alpha_{xx} + \alpha_{yy} + \alpha_{zz}\right) \quad (6)$$

$$\beta_0 = \left(\beta_x^2 + \beta_y^2 + \beta_z^2\right)^{1/2} \quad (7)$$

Hyperpolarizability

Doping the surface of C_3N_4 with Cu, Ag, and Au lowered the cocoon and is predicted to display significant nonlinear and optoelectronic response. All investigated compounds' mean first hyperpolarizability (β_O), and their components (x, y, and z) has been analyzed as presented in Table 7**.** Pure surface C_3N_4 has a static hyperpolarizability of 269.51 au, however after doping, it dramatically rises as seen in the Fig. 15. All of the transition metal doped complexes in this work showed great hyperpolarizabilities and would display wonderful optoelectronic capabilities, as was discovered.

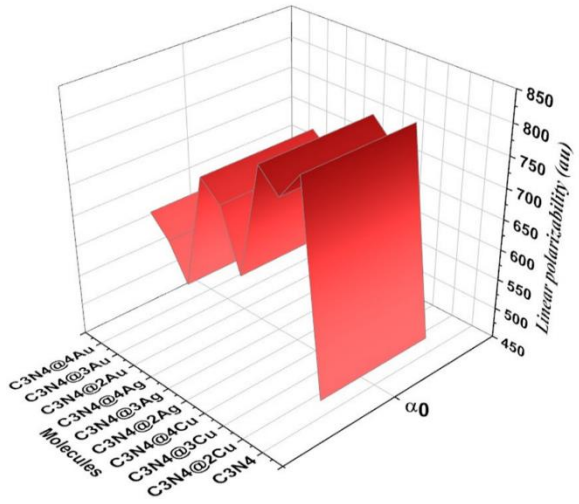

Fig. 14: Graphical depiction of linear polarizability or static mean polarizability(α_O) of researched structures.

Table-7: Computed first hyperpolarizabilities of all the studied compounds and their x, y and z components.

Compounds	β_x	β_y	β_z	β_{tot}
C_3N_4	-75.18	-0.01	-258.81	269.51
C_3N_4@2Cu	-66631.47	60477.66	-27859.20	94198.91
C_3N_4@3Cu	128048.68	57105.43	-3377.00	140245.86
C_3N_4@4Cu	-54804.990	75190.23	48515.86	104933.05
C_3N_4@2Ag	-57943.36	-92.30	123531.10	136445.49
C_3N_4@3Ag	-34723.975	25994.68	5868.61	43771.21
C_3N_4@4Ag	71605.60	32745.61	52655.40	94721.85
C_3N_4@2Au	643.04	107.19	-299.54	717.45
C_3N_4@3Au	945.57	1130.01	102.0026	1298.65
C_3N_4@4Au	1806.25	2239.71	1094.47	3078.43

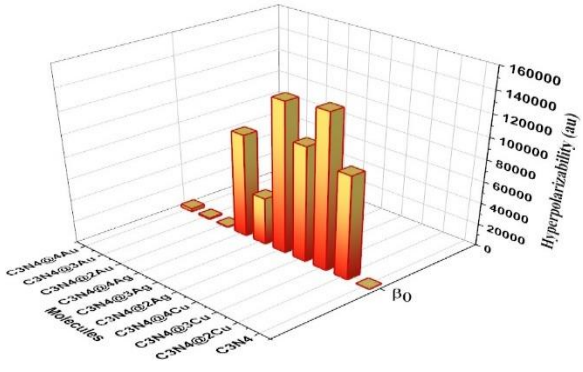

Fig. 15: Graphical depiction of β_O of researched structures

The two-level model is characterized by Eq. 8 [58-60];

$$\beta_0 \propto \Delta\mu \times f_{osc} / \Delta E^3 \quad (8)$$

According to the Eq. 8, all proposed complexes had increased β_O due to greater $\Delta\mu$ and lower ΔE than C_3N_4 (see Fig. 16).
It can be seen that β_O value alters with $f_{osc} / \Delta E^3$ value (Table 8).

Table-8: α_O, β_O, $\Delta\mu$ and $f_{osc} / \Delta E^3$ of investigated compounds.

Compounds	α_0(au)	β_0(au)	Δμ (au)	$f_{osc} / \Delta E^3$
C_3N_4	479.00	269.51	0.5104	0.0002
C_3N_4@2Cu	809.99	94198.91	2.2656	0.0372
C_3N_4@3Cu	762.78	140245.86	3.8145	0.0754
C_3N_4@4Cu	795.45	104933.05	1.9766	0.0661
C_3N_4@2Ag	608.98	136445.49	0.5899	0.0021
C_3N_4@3Ag	704.76	43771.21	1.4201	0.0754
C_3N_4@4Ag	732.78	94721.85	1.5734	0.0014
C_3N_4@2Au	541.81	717.45	0.6790	0.0004
C_3N_4@3Au	598.65	1298.65	1.1437	0.0026
C_3N_4@4Au	630.91	3078.43	1.1337	0.0064

Electrical conductivity (Б)

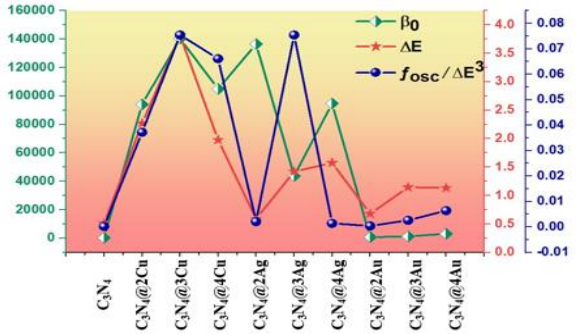

Fig. 16: Graphical view of β_O in relation with the oscillator strength (f_{osc}), excitation energy (ΔE) and $f_{osc} / \Delta E^3$ of all researched structures.

The electrical conductivity (Б) of doped compounds with NLO characteristics is predicted most accurately by E_g. The unique compounds resemble semiconductors more due to their narrow E_g. Hence, compared to undoped C_3N_4, it is predicted that the Б is increased.

Eq. 9 [61] has been employed to calculate Б.

$$Б \propto exp\left(\frac{-E_g}{2kT}\right) \quad (9)$$

Б, the E_g, the Boltzmann constant k, and temperature T in kelvin are all included in the equation [62]. According to our investigation, the electrical conductivities of all new complexes are much higher than those of undoped C_3N_4. Our suggested doped complexes may therefore serve as ground-breaking sensing materials.

Conclusion

In this study, nine novel C_3N_4-based compounds—namely C_3N_4@2Cu, C_3N_4@3Cu, C_3N_4@4Cu, C_3N_4@2Ag, C_3N_4@3Ag, C_3N_4@4Ag, C_3N_4@2Au, C_3N_4@3Au, and C_3N_4@4Au—were designed via a systematic metal doping approach using copper (Cu), silver (Ag), and gold (Au) atoms in varying concentrations. Theoretical investigations were carried out at the B3LYP/LANL2DZ level of theory to explore the electronic and optical properties of these systems. Key nonlinear optical (NLO) and optoelectronic parameters were evaluated to assess their performance potential in advanced material applications. Compared to pristine C_3N_4 (Eg = 3.50 eV, λ_max = 383 nm, ΔE = 3.23 eV, α_0 = 479.00 au, β_0 = 479.10 au), all doped complexes demonstrated substantial enhancements. The predicted properties for the doped systems include red-shifted absorption maxima (λ_max = 438–836 nm), significantly reduced energy gaps (Eg = 0.63–2.29 eV), lowered transition energies (ΔE = 1.39–2.99 eV), and improved transition dipole moments (Δμ = 0.6790–3.8145 au). Furthermore, the static mean polarizabilities (α_0) ranged from 541.81 to 809.99 au, while the mean first hyperpolarizabilities (β_0) spanned a broad range from 717.45 to 140,245.86 au. Isotropic (α_iso) and anisotropic (α_aniso) polarizabilities were also found to lie between 541.81–809.99 au and 407.40–1298.65 au, respectively. These findings indicate that the proposed doped C_3N_4 materials exhibit promising NLO and optoelectronic characteristics, far surpassing those of the undoped system. The results offer valuable insights into the future synthesis of excess-electron-type molecular systems and could serve as a

theoretical foundation for the design of high-performance NLO materials.

Acknowledgment

The experiments presented in this paper were partially carried out using the facilities of the Benefit Advanced AI and Computing Lab at the University of Bahrain (https://ailab.uob.edu.bh) with support from Benefit Bahrain Company (https://benefit.bh).

References

1. Canioni, M. Bellec, A. Royon, B. Bousquet and T. Cardinal, Three-dimensional optical data storage using third-harmonic generation in silver zinc phosphate glass, *Opt. Lett*., **33**, 360 (2008).
2. Z. R. Khan, M. Shkir, V. Ganesh, S. AlFaify, I. S. Yahia and H. Y. Zahran, Linear and nonlinear optics of CBD grown nanocrystalline F doped CdS thin films for optoelectronic applications: an effect of thickness, *J. Electron. Mater*., **47**, 5386 (2018).
3. R. Rajkumar and P. P. Kumar, Structure, crystal growth and characterization of piperazinium bis (4-nitrobenzoate) dihydrate crystal for nonlinear optics and optical limiting applications, *J. Mol. Struct*., **1179**, 108 (2019).
4. M. Homocianu, A. Airinei, C. Hamciuc and A. M. Ipate, Nonlinear optical properties (NLO) and metal ions sensing responses of a polymer containing 1,3,4-oxadiazole and bisphenol A units, *J. Mol. Liq*., **281**, 141 (2019).
5. F. Huo, H. Zhang, Z. Chen, L. Qiu, J. Liu, S. Bo and I. V. Kityk, Novel nonlinear optical push–pull fluorene dyes chromophore as promising materials for telecommunications, *J. Mater. Sci. Mater. Electron*., **30**, 12180 (2019).
6. V. P. Ananikov, Organic–inorganic hybrid nanomaterials, Nanomaterials, **9**, 1197 (2019).
7. A. R. Ayub, R. A. Shehzad, S. S. Alarfaji and J. Iqbal, Super alkali (OLi_3) doped boron nitride with enhanced nonlinear optical behavior, *J. Nonlinear Opt. Phys. Mater*., **29**, 2050004 (2020).
8. I. Khan, M. Khalid, M. Adeel, S. I. Niaz, I. Shafiq, S. Muhammad and A. A. C. Braga, Palladium-catalyzed synthesis of 5-(arylated) pyrimidines, their characterization, electronic communication, and non-linear optical evaluations, *J. Mol. Struct*., **1237**, 130408 (2021).
9. A. Irfan, M. Pannipara, A. G. Al-Sehemi, M. W. Mumtaz, M. A. Assiri, A. R. Chaudhry and S. Muhammad, Exploring the effect of electron withdrawing groups on optoelectronic properties of pyrazole derivatives as efficient donor and acceptor materials for photovoltaic devices, *Z. Phys. Chem*., **233**, 1625 (2019).
10. D. Xiao, F. A. Bulat, W. Yang and D. N. Beratan, A donor−nanotube paradigm for nonlinear optical materials, *Nano Lett*., **8**, 2814 (2008).
11. M. J. Lee, M. Piao, M. Y. Jeong, S. H. Lee, K. M. Kang, S. J. Jeon and B. R. Cho, Novel azo octupoles with large first hyperpolarizabilities, *J. Mater. Chem*., **13**, 1030 (2003).
12. V. Parthasarathy, R. Pandey, P. K. Das, F. Castet and M. Blanchard-Desce, Linear and nonlinear optical properties of tricyanopropylidene-based merocyanine dyes: synergistic experimental and theoretical investigations, *ChemPhysChem*, **19**, 187 (2018).
13. H. Zhang, Y. Tian, S. Bo, L. Xiao, Y. Ao, J. Zhang and M. Li, A study on regulating the conjugate position of NLO chromophores for reducing the dipole moment and enhancing the electro-optic activities of organic materials, *J. Mater. Chem. C*, **8**, 1380 (2020).
14. T. Michinobu and F. Diederich, The [2+2] cycloaddition-retroelectrocyclization (CA-RE) click reaction: facile access to molecular and polymeric push-pull chromophores, *Angew. Chem. Int. Ed*., **57**, 3552 (2018).
15. Z. Liu, S. Hua and G. Wu, Extended first hyperpolarizability of quasi-octupolar molecules by halogenated methylation: whether the iodine atom is the best choice, *J. Phys. Chem.* C, **122**, 21548 (2018).
16. Y. Li, Z. R. Li, D. Wu, R. Y. Li, X. Y. Hao and C. C. Sun, An ab initio prediction of the extraordinary static first hyperpolarizability for the electron-solvated cluster $(FH)_2^-(HF)$, *J. Phys. Chem.* B, **108**, 3145 (2004).
17. W. Chen, Z. R. Li, D. Wu, F. L. Gu, X. Y. Hao, B. Q. Wang, C. C. Sun, The static polarizability and first hyperpolarizability of the water trimer anion: ab initio study, *J. Chem. Phys*., **121**, 10489 (2004).
18. A. Rasool, S. Zahid, N. Alfryyan, A. R. Ayub, K. Ayub, M. S. Akhter and E. S. Yousef, Remarkable non-linear optical properties of gold cluster doped graphyne (GY): a DFT study, *J. Mol. Graph. Model*., **114**, 108204 (2022).
19. F. Khaliq, K. Ayub, T. Mahmood, S. Muhammad, S. Tabassum and M. A. Gilani, First example of lanthanum as dopant on $Al_{12}N_{12}$ and $Al_{12}P_{12}$ nanocages for improved electronic and nonlinear optical properties with high stability, *Mater. Sci. Semicond. Process*., **135**, 106122 (2021).2.
20. A. Ahsin and K. Ayub, Remarkable electronic and NLO properties of bimetallic superalkali clusters: a DFT study, *J. Nanostruct. Chem*., **12**, 529 (2022).

21. Z. J. Li, F. F. Wang, Z. R. Li, H. L. Xu, X. R. Huang, D. Wu and Y. Aoki, Large static first and second hyperpolarizabilities dominated by excess electron transition for radical ion pair salts $M^{2+}TCNQ^{-}$
22. G. Yu, X. Huang, S. Li, W. Chen, Theoretical insights and design of intriguing nonlinear optical species involving the excess electron, *Int. J. Quantum Chem*., **115**, 671 (2015).
23. J. Iqbal, R. Ludwig and K. Ayub, Phosphides or nitrides for better NLO properties? A detailed comparative study of alkali metal doped nano-cages, *Mater. Res. Bull*., **92**, 113 (2017).
24. W. M. Sun, L. T. Fan, Y. Li, J. Y. Liu, D. Wu andZ. R. Li, On the potential application of superalkali clusters in designing novel alkalides with large nonlinear optical properties, *Inorg. Chem*., **53**, 6170 (2014).
25. J. Xu, L. Zhang, R. Shi and Y. Zhu, Chemical exfoliation of graphitic carbon nitride for efficient heterogeneous photocatalysis, *J. Mater. Chem*. A, **1**, 14766 (2013).
26. K. Schwinghammer, M. B. Mesch, V. Duppel, C. Ziegler, J. Senker and B. V. Lotsch, Crystalline carbon nitride nanosheets for improved visible-light hydrogen evolution, *J. Am. Chem. Soc*., **136**, 1730 (2014).
27. F. Goettmann, A. Fischer, M. Antonietti and A. Thomas, Metal-free catalysis of sustainable Friedel–Crafts reactions: direct activation of benzene by carbon nitrides to avoid the use of metal chlorides and halogenated compounds, *Chem. Commun*., **43**, 4530 (2006).
28. X. Liu, R. Ma, L. Zhuang, B. Hu, J. Chen, X. Liu and X. Wang, Recent developments of doped g-C_3N_4 photocatalysts for the degradation of organic pollutants, *Crit. Rev. Environ. Sci. Technol.*, **51**, 751 (2021).
29. H. Murthy, Graphitic carbon nitride (GCN) for solar cell applications, Nanoscale Graphitic Carbon Nitride, 225 (2022).
30. X. Liu, R. Ma, L. Zhuang, B. Hu, J. Chen, X. Liu and X. Wang, Recent developments of doped g-C_3N_4 photocatalysts for the degradation of organic pollutants, *Crit. Rev. Environ. Sci. Technol.*, **51**, **8**, 751 (2021).
31. Y. Zhang, Y. Zhao and Y. Zhu, Enhanced visible-light photocatalytic activity of Ag-modified g-C_3N_4, *Appl. Surf. Sci*., 506, 144924 (2020).
32. A. Rasool, H. Yousaf and U. Mehmood, Remarkable NLO properties of gold cluster doped graphyne: A DFT study, *J. Mol*. Graph. Model., **113**, 108084 (2022)
33. J. Li, H. Wang and Y. Sun, Electronic structure and photocatalytic behavior of Cu-doped g-C_3N_4: A DFT investigation, *ChemPhysChem,* **22**, 1323 (2021).
34. X. Liu, Y. Jin and W. Liu, Recent developments of doped g-C_3N_4 photocatalysts: preparation, modification, and applications, *Crit. Rev. Environ. Sci. Technol.*, **51**, 2109 (2021).
35. M. J. Frisch and E. A. Johnson, Gaussian 09, Revision D.01, Gaussian Inc., Wallingford CT, 201 (2009).
36. M. Shamim, M. Perveen, S. Nazir, M. Hussnain, R. Mehmood, M. I. Khan and J. Iqbal, DFT study of therapeutic potential of graphitic carbon nitride (g-C_3N_4) as a new drug delivery system for carboplatin to treat cancer, *J. Mol. Liq*., **331**, 115607 (2021).
37. M. Perveen, S. Nazir, A. W. Arshad, M. I. Khan, M. Shamim, K. Ayub and J. Iqbal, Therapeutic potential of graphitic carbon nitride as a drug delivery system for cisplatin (anticancer drug): a DFT approach, *Biophys. Chem*., **267**, 106461 (2020).
38. R. Dennington, T. A. Keith and J. M. Millam, GaussView 6.0.16, Semichem Inc., Shawnee Mission, KS, USA, 143 (2016).
39. T. Lu, F. Chen, Multiwfn: a multifunctional wavefunction analyzer, *J. Comput. Chem*., **33**, 580 (2012).
40. S. I. Gorelsky, SWizard Program, University of Ottawa, Ottawa, Canada (2010).
41. L. A. Deschenes and D. A. Vanden Bout, Origin 6.0: Scientific Data Analysis and Graphing Software, Origin Lab Corporation, www.originlab.com (2000).
42. Y. Arshad, S. Khan, M. A. Hashmi and K. Ayub, Transition metal doping: a new and effective approach for remarkably high nonlinear optical response in aluminum nitride nanocages, *New J. Chem*., **42**, 6976 (2018).
43. S. Zahid, A. Rasool, A. R. Ayub, K. Ayub, J. Iqbal, M. S. Al-Buriahi and H. H. Somaily, Silver cluster doped graphyne (GY) with outstanding non-linear optical properties, *RSC Adv.*, **12**, 5466 (2022).
44. N. Maqsood, A. Asif, A. Elmushyakhi, M. Ans, R. A. Shehzad, A. Rasool and J. Iqbal, Environmentally affable and highly efficient donor material based on cyclopentadithiophene (CPDT) framework for remarkable organic solar cells, *Opt. Mater*., **135**, 113316 (2023).
45. A. Perez-Gonzalez, A. Galano and J. V. Ortiz, Vertical ionization energies of free radicals and electron detachment energies of their anions: a comparison of direct and indirect methods versus experiment, *J. Phys. Chem.* A, **118**, 6125 (2014).
46. N. Maqsood, A. Asif, K. Ayub, J. Iqbal, A. Y. Elnaggar, G. A. Mersal and S. M. El-Bahy, DFT

study of alkali and alkaline earth metal-doped benzocryptand with remarkable NLO properties, *RSC Adv*., **12**, 16029 (2022).

47. A. S. Rad and K. Ayub, Nonlinear optical and electronic properties of Cr-, Ni-, and Ti-substituted C_{20} fullerenes: a quantum-chemical study, *Mater. Res. Bull*., **97**, 399 (2018).
48. F. Ullah, N. Kosar, A. Ali, T. Mahmood and K. Ayub, Design of novel inorganic alkaline earth metal doped aluminum nitride complexes ($AEM@Al_{12}N_{12}$) with high chemical stability, improved electronic properties and large nonlinear optical response, *Optik*, **207**, 163792 (2020).
49. A. Hussain, N. M. A. Hadia, M. M. Hessien, R. A. Khera, S. Zahid, R. A. Shehzad and J. Iqbal, DFT study of super-halogen (Al_7) doped carbon nitride (C_2N) and its nonlinear optical properties, *J. Mol. Struct*., **1270**, 133910 (2022).
50. A. Rafique, H. Maqbool, R. A. Shehzad, I. A. Bhatti and K. Ayub, A. Elmushyakhi, J. Iqbal, DFT study of enhancement in nonlinear optical response of exohedrally and endohedrally alkaline earth metals (Be, Mg, Ca) doped adamanzane, *Int. J. Quantum Chem*., **123**, e27060 (2023).
51. H. Maqbool, A. Rafique, I. A. Bhatti, A. M. Shawky, K. Ayub and J. Iqbal, Novel endohedrally and exohedrally metals (Li, Na, K, Ag) doped (15-crown-5) with remarkable electronic, static and dynamic NLO response, Optik, **271**, 170169 (2022).
52. M. U. Khan, M. Ibrahim, M. Khalid, M. S. Qureshi, T. Gulzar, K. M. Zia and M. R. S. A. Janjua, First theoretical probe for efficient enhancement of nonlinear optical properties of quinacridone based compounds through various modifications, *Chem. Phys. Lett*., **715**, 222 (2019).
53. M. U. Khan, M. Khalid, M. N. Arshad, M. N. Khan, M. Usman, A. Ali and B. Saifullah, Designing star-shaped subphthalocyanine-based acceptor materials with promising photovoltaic parameters for non-fullerene solar cells, *ACS Omega*, **5**, 23039 (2020).
54. L. Wang, J. T. Ye, H. Q. Wang, H. M. Xie and Y. Q. Qiu, Self-assembled donor–acceptor chromophores: evident layer effect on the first hyperpolarizability and two-dimensional charge transfer character, *J. Phys. Chem. C*, **121**(39), 21616 (2017).
55. W. Y. Wang, N. N. Ma, S. L. Sun and Y. Q. Qiu, Redox control of ferrocene-based complexes with systematically extended π-conjugated connectors: switchable and tailorable second order nonlinear optics, *Phys. Chem. Chem. Phys*., **16**, 4900 (2014).
56. A. Karakas, A. Elmali and H. Unver, Linear optical transmission measurements and computational study of linear polarizabilities, first hyperpolarizabilities of a dinuclear iron (III) complex, *Spectrochim. Acta A Mol. Biomol. Spectrosc*., **68**, 567 (2007).
57. M. R. S. A. Janjua, C. G. Liu, W. Guan, J. Zhuang, S. Muhammad, L. K. Yan and Z. M. Su, Prediction of remarkably large second-order nonlinear optical properties of organoimido-substituted hexamolybdates, J. Phys. Chem. A, **113**(15), 3576–3587 (2009).
58. H. Sajid, F. Ullah, S. Khan, K. Ayub, M. Arshad and T. Mahmood, Remarkable static and dynamic NLO response of alkali and superalkali doped macrocyclic [hexa-] thiophene complexes; a DFT approach, RSC Adv., **11**(7), 4118–4128 (2021).
59. X. Li, Design of novel graphdiyne-based materials with large second-order nonlinear optical properties, J. Mater. Chem. C, **6**(28), 7576–7583 (2018).
60. N. Hou, F. Y. Du, R. Feng, H. S. Wu and Z. R. Li, Effects of the atomic number of alkali atom and pore size of graphyne on the second-order nonlinear optical response of superalkali salts of graphynes $OM_3^+@GYs^-$ (M = Li, Na, and K), Int. J. Quantum Chem., **121**(4), e26477 (2021).
61. X. Li and J. Lu, Giant enhancement of electronic polarizability and the first hyperpolarizability of fluoride-decorated graphene versus graphyne and graphdiyne: insights from ab initio calculations, Phys. Chem. Chem. Phys., **21**(24), 13165–13175 (2019).
62. L. Ma, J. M. Zhang, K. W. Xu and V. Ji, A first-principles study on gas sensing properties of graphene and Pd-doped graphene, Appl. Surf. Sci., 343, 121–127 (2015).